A stabilization-free Virtual Element Method based on divergence-free projections

Computer Methods in Applied Mechanics and Engineering 424 (2024) 116885

Contents lists available at ScienceDirect

Comput. Methods Appl. Mech. Engrg.

journal homepage: www.elsevier.com/locate/cma

A stabilization-free Virtual Element Method based on divergence-free projections

Stefano Berrone, Andrea Borio, Francesca Marcon *

Dipartimento di Scienze Matematiche, Politecnico di Torino, Corso Duca degli Abruzzi 24, Torino, 10129, TO, Italy

ARTICLE INFO

MSC:
65N12
65N15
65N30

Keywords:
Virtual element methods
Poisson problem
Polygonal meshes

ABSTRACT

In this paper, we propose and analyze a Stabilization Free Virtual Element Method (SFVEM), that allows the definition of bilinear forms that do not require an arbitrary stabilization term, thanks to the exploitation of higher-order polynomial projections on divergence free vectors of polynomials. The method is introduced in the lowest order formulation for the Poisson problem. We provide a sufficient condition on the polynomial projection space that implies the well-posedness, proved on particular classes of polygons, and optimal order a priori error estimates. Numerical tests on convex and non-convex polygonal meshes confirm the theoretical convergence rates and show that the method is suitable for solving problems characterized by anisotropies.

1. Introduction

In recent years, the study of polygonal methods for solving partial differential equations has received a huge attention. The main reason for this great interest relies in the flexibility of polygonal meshes to discretize domains with high geometrical complexity. One of the most recent developments in this field is the family of the Virtual Element Methods (VEM). These methods were first introduced in primal conforming form in [1] and were later on applied to most of the relevant problems of interest in applications.

Standard VEM discrete bilinear forms are the sum of a singular part maintaining consistency on polynomials and a stabilizing form enforcing coercivity. In the literature, the stabilization term has been extensively studied, for instance in [2], and remains a somehow arbitrarily chosen component of the method with several possible effects on the stability and conditioning of the method. Due to the issues that can be caused by the arbitrary choice of the stabilization (see for instance SUPG stabilizations [3,4], multigrid analysis [5], complex non-linear problems [6]), in the last years the idea of proposing a new VEM formulation that does not require an arbitrary non-polynomial stabilization has grown. In [7] the so called Enlarged Enhancement Virtual Element Method (E^2VEM) was proposed, based the definition of bilinear forms that involves only polynomial projections. This method is based on the exploitation of higher order polynomial projections that are made computable by suitably enlarging the enhancement property of local virtual spaces, without modifying the degrees of freedom. The degree of polynomial enrichment is chosen locally on each polygon, such that the discrete bilinear form is coercive, and depends on the geometry of the polygon. The definition of a VEM scheme based on higher order polynomial projections has been studied numerically and applied in many different contexts, and in particular on elasticity problems [8–11], in the study of eigenvalue problems [12], in case of convection-dominated problems [13] and on problems characterized by anisotropies [7]. Numerical results show that a stabilization-free formulation can speed up convergence in the case of anisotropic diffusion tensors, and can reduce the magnitude of the error in some situations, in general being never worse than the standard one. In [14], in the context of a comparison between the proposed method and standard Virtual Elements [15], a stabilization free

* Corresponding author.
E-mail addresses: stefano.berrone@polito.it (S. Berrone), andrea.borio@polito.it (A. Borio), francesca.marcon@polito.it (F. Marcon).

https://doi.org/10.1016/j.cma.2024.116885
Received 4 December 2023; Received in revised form 1 February 2024; Accepted 26 February 2024

method that involves projection operators defined on spaces of harmonic polynomials was proposed. This scheme can be defined without changing the definition of the VEM space. Similarly, in [16] a mixed SFVEM scheme was proposed and theoretically studied for the particular case of quadrilaterals. At the meantime, other Virtual Element schemes for which no stabilization form is required have been recently presented in [17,18] and new studies about the stabilization have been proposed in [19,20].

In this work, we propose a new Stabilization Free Virtual Element Methods (SFVEM), designed to allow the definition of a coercive bilinear form that involves higher order polynomial projections with respect to the standard one [15], while the original discrete space is untouched. In particular, we prove explicitly that on general quadrilateral elements the projection of gradients of VEM functions in the space of curls of quadratic harmonic polynomials is a coercive operator. Regarding more general geometries, we identify sufficient conditions that the local polynomial space has to satisfy such that the gradient projection is coercive. These conditions can be verified numerically in the projection construction to build a coercive projection of VEM gradients that is a divergence-free polynomial. Moreover, we provide explicit sufficient conditions for convex polygons, polygons with one concavity and an edge belonging to their kernel, and polygons with arbitrary number of aligned edges whose boundary lies on exactly three straight lines.

For the sake of simplicity, we focus on the two dimensional Poisson's problem with homogeneous Dirichlet boundary conditions, the extension to general boundary conditions and more general second order elliptic problems being analogous to what is done for classical VEM, since the results about the projection of gradients depend only on the element's geometry and not on the operator. Moreover, the formulation and proofs presented in this work can also be easily extended to the case of a non constant anisotropic diffusion tensor.

The outline of the paper is as follows. In Section 2 we state our model problem. In Section 3 we introduce the approximation functional spaces and projection operators and we state the discrete problem. Section 4 contains the theoretical results about the well-posedness. In Section 5 we present optimal order H^1 and L^2 a priori error estimates. Section 7 contains some numerical results assessing the stability of the method and confirming the predicted rates of convergence, as well as some comparisons with standard VEM schemes. Finally, Appendix contains some theoretical results about sufficient projection degrees for certain classes of polygons.

Throughout the work, $(\cdot,\cdot)_\omega$ denotes the standard L^2 scalar product defined on a generic $\omega \subset \mathbb{R}^2$, $\|\cdot\|_\omega$ denotes the corresponding norm, $\gamma^{\partial\omega}$ denotes the trace operator, that restricts on the boundary $\partial\omega$ an element of a space defined over $\omega \subset \mathbb{R}^2$. Inside the proofs, the symbol C denotes any constant, independent of the mesh size.

2. Model problem

Let $\Omega \subset \mathbb{R}^2$ be a bounded open set. We are interested in solving the following problem:

$$\begin{cases} -\Delta u = f & \text{in } \Omega, \\ u = 0 & \text{on } \partial\Omega. \end{cases} \tag{1}$$

Assuming $f \in L^2(\Omega)$, the variational formulation of (1) is given by: find $u \in H_0^1(\Omega)$ such that,

$$(\nabla u, \nabla v)_\Omega = (f, v)_\Omega \quad \forall v \in H_0^1(\Omega). \tag{2}$$

3. Discrete formulation

Let $\mathcal{M}_h$ denote a conforming polygonal tessellation of Ω and $E \in \mathcal{M}_h$ denotes a generic polygon. Let h_E denote the diameter of each $E \in \mathcal{M}_h$ and $h := \max_{E\in\mathcal{M}_h} h_E$. Let $\{V_i\}_{i=1}^{N_E}$ be the N_E vertices of E clockwise ordered, $\mathcal{E}_E$ the set of its edges and $\boldsymbol{n}^{e_i} = (n_x^{e_i}, n_y^{e_i})$ the outward-pointing unit normal vector to the edge e_i of E, which links the vertex V_i to the vertex V_{i+1} (with the usual notation $V_{N_E+1} \equiv V_1$). We assume that $\mathcal{M}_h$ satisfies the standard mesh assumptions for VEM (see for instance [2,21]), i.e. $\exists\kappa > 0$ such that

A.1 for all $E \in \mathcal{M}_h$, E is star-shaped with respect to a ball of radius $\rho \geq \kappa h_E$;
A.2 for all edges $e \in \mathcal{E}_E$, $|e| \geq \kappa h_E$.

For any given $E \in \mathcal{M}_h$, let $\mathbb{P}_k(E)$ be the space of polynomials of degree up to k defined on E. Let $\Pi_1^{\nabla,E} : H^1(E) \to \mathbb{P}_1(E)$ be the $H^1(E)$-orthogonal projection defined up to a constant by the orthogonality condition:

$$\forall u \in H^1(E), \quad \left(\nabla\left(\Pi_1^{\nabla,E}u - u\right), \nabla p\right)_E = 0 \ \ \forall p \in \mathbb{P}_1(E). \tag{3}$$

In order to define $\Pi_1^{\nabla,E}$ uniquely, we set $\int_{\partial E} \gamma^{\partial E}\left(\Pi_1^{\nabla,E}u\right) = \int_{\partial E} \gamma^{\partial E}(u)$. In the following, for the sake of simplicity we omit the trace operator γ when it is clear from the integration domain.

For any given $E \in \mathcal{M}_h$, let $\mathcal{V}_{h,1}^E$ be the local Virtual Element Space of order 1:

$$\begin{aligned} \mathcal{V}_{h,1}^E := \{ & v \in H^1(E) : \ \Delta v \in \mathbb{P}_1(E), \ \ \gamma^e(v) \in \mathbb{P}_1(e) \ \forall e \in \mathcal{E}_E, \ \ v \in C^0(\partial E) \\ & (v,p)_E = \left(\Pi_1^{\nabla,E}v, p\right)_E \ \ \forall p \in \mathbb{P}_1(E)\}. \end{aligned}$$

We recall that the degrees of freedom of this space are the values of functions at the vertices of E (see [15,22]). Moreover, we define the global discrete space as

$$\mathcal{V}_{h,1} := \{v \in H_0^1(\Omega) : v_{|E} \in \mathcal{V}_{h,1}^E\}.$$

To define our local discrete bilinear form, for any given $E \in \mathcal{M}_h$, let $\ell_E \in \mathbb{N}$ be given, as detailed in the following, where we will choose ℓ_E depending on E.

Let $\hat{\Pi}^{0,E}_{\ell_E}\nabla : \mathrm{H}^1(E) \to \mathbf{curl}\,\mathbb{P}_{\ell_E+1}(E)$ be the $\mathrm{L}^2(E)$-projection operator of the gradient of functions in $\mathrm{H}^1(E)$, defined, $\forall u \in \mathrm{H}^1(E)$, by the orthogonality condition

$$\left(\hat{\Pi}^{0,E}_{\ell_E}\nabla u, \mathbf{curl}\, p\right)_E = (\nabla u, \mathbf{curl}\, p)_E \quad \forall p \in \mathbb{P}_{\ell_E+1}(E)\,, \tag{4}$$

where for any $p \in \mathbb{P}_{\ell_E+1}(E)$, $\mathbf{curl}\, p = \left(\frac{\partial p}{\partial y}, -\frac{\partial p}{\partial x}\right)$. Notice that for any $p \in \mathbb{P}_{\ell_E+1}(E)$, $\mathbf{curl}\, p = \mathbf{0}$ if and only if p is constant.

For each function $u_h \in \mathcal{V}^E_{h,1}$, the above projection is computable given the degrees of freedom of u_h applying the Gauss–Green formula, indeed $\forall p \in \mathbb{P}_{\ell_E+1}(E)$ we have, thanks to known results about De Rham diagrams in Sobolev spaces, see e.g. [23]

$$\left(\nabla u_h, \mathbf{curl}\, p\right)_E = \left(\nabla u_h \cdot \boldsymbol{t}^{\partial E}, p\right)_{\partial E}\,. \tag{5}$$

Remark 1. It can be easily seen that, thanks to Schwartz theorem,

$$\mathbf{curl}\,\mathbb{P}_{\ell_E+1}(E) = \{\boldsymbol{p} \in \left[\mathbb{P}_{\ell_E}(E)\right]^2 : \nabla \cdot \boldsymbol{p} = 0\}.$$

Moreover, it holds $\nabla\mathbb{P}_1(E) = \mathbf{curl}\,\mathbb{P}_1(E)$.

Let $a^E_h : \mathrm{H}^1(E) \times \mathrm{H}^1(E) \to \mathbb{R}$ be defined as

$$a^E_h\left(u_h, v_h\right) := \left(\hat{\Pi}^{0,E}_{\ell_E}\nabla u_h, \hat{\Pi}^{0,E}_{\ell_E}\nabla v_h\right)_E \quad \forall u_h, v_h \in \mathrm{H}^1(E)\,, \tag{6}$$

and $a_h : \mathrm{H}^1(\Omega) \times \mathrm{H}^1(\Omega) \to \mathbb{R}$ as

$$a_h\left(u_h, v_h\right) := \sum_{E\in\mathcal{M}_h} a^E_h\left(u_h, v_h\right) \quad \forall u_h, v_h \in \mathrm{H}^1(\Omega)\,. \tag{7}$$

We can state the discrete problem as: find $u_h \in \mathcal{V}_{h,1}$ such that

$$a_h\left(u_h, v_h\right) = \sum_{E\in\mathcal{M}_h} \left(f, \Pi^{0,E}_0 v_h\right)_E \quad \forall v_h \in \mathcal{V}_{h,1}\,, \tag{8}$$

where $\Pi^{0,E}_0 v_h = \frac{1}{|E|}\int_E v_h$, computable by standard VEM techniques [24].

4. Well-posedness

This section is devoted to prove the well-posedness of the discrete problem stated by (8). First we focus on the proof of the continuity and the coercivity of the local discrete bilinear form a^E_h defined in (6), which implies that the bilinear form a_h of the problem (8) satisfies the hypotheses of the Lax–Milgram theorem. Then, in Section 4.3 we prove the coercivity of the global discrete problem (8) with respect to the $\mathrm{H}^1_0(\Omega)$ norm.

In Proposition 1, we prove the continuity of the local discrete bilinear form a^E_h defined in (6). The proof of the coercivity of the local discrete bilinear form a^E_h is split in two cases. First, in Section 4.1 (Theorem 1), we prove the coercivity in the case of quadrilaterals, showing that the gradient projection in the space of curls of quadratic harmonic polynomials is coercive. In Section 4.2, for each $E \in \mathcal{M}_h$ with $N_E \geq 5$, we provide a sufficient condition on the polynomial projection space that implies the coercivity. In Appendix we provide proofs of the validity of this sufficient condition for some classes of polygons. We omit the proof of the coercivity if E is a triangle ($N_E = 3$ and $\ell_E = 0$), indeed in this case $\mathcal{V}^E_{h,1} = \mathbb{P}_1(E)$ and then $\hat{\Pi}^{0,E}_0\nabla v_h = \nabla v_h$.

Proposition 1. *For every $E \in \mathcal{M}_h$, the discrete bilinear form a^E_h defined by (6) satisfies*

$$a^E_h\left(u_h, v_h\right) \leq \left\|\nabla u_h\right\|_E \left\|\nabla v_h\right\|_E \quad \forall u_h, v_h \in \mathcal{V}^E_{h,1}\,. \tag{9}$$

The proof can be derived immediately applying the definition of $\hat{\Pi}^{0,E}_{\ell_E}$ and the Cauchy–Schwarz inequality.

4.1. Local coercivity for $N_E = 4$

In this section we focus on the case $N_E = 4$ and we follow an approach similar to the one used in [16]. We choose $\ell_E = 1$, so that $\hat{\Pi}^{0,E}_1\nabla$ projects onto the space of **curl** of quadratic polynomials, see (4).

Let $\xi_h \in \mathcal{V}^E_{h,1}$ be defined such that

$$\xi_h(V_i) = (-1)^i \quad \forall i = 1, \dots, 4\,, \tag{10}$$

then we introduce the virtual space

$$\mathrm{H}(E) := \mathrm{span}(\xi_h) \subset \mathcal{V}^E_{h,1}\,. \tag{11}$$

Notice that $\mathrm{H}(E)$ is a one dimensional space and that $\xi_h \notin \mathbb{P}_1(E)$, in fact by definition (10) $\int_e \xi_h = 0$ for each edge $e \subset \partial E$, then

$$\left(\nabla\xi_h, \nabla p_1\right)_E = \left(\xi_h, \nabla p_1 \cdot \boldsymbol{n}^{\partial E}\right)_{\partial E} = \sum_{e\subset\partial E} \nabla p_1 \cdot \boldsymbol{n}^e \int_e \xi_h = 0\,. \tag{12}$$

Then $\mathrm{H}(E)$ is $\mathrm{H}^1(E)$-orthogonal to $\mathbb{P}_1(E)$ and

$$\mathcal{V}_{h,1}^E = \mathbb{P}_1(E) \oplus \mathrm{H}(E)\,, \tag{13}$$

i.e. any function $v_h \in \mathcal{V}_{h,1}^E$ can be uniquely written as $v_h = p_1 + c\,\xi_h$, for some polynomial $p_1 \in \mathbb{P}_1(E)$ and some constant $c \in \mathbb{R}$. Finally, from the boundedness of the norms of gradients of standard VEM basis functions (see [25, Lemma 4.9]), we immediately obtain that there exists $C_{\xi_h} > 0$, independent of h_E, such that

$$\left\|\nabla\xi_h\right\|_E \le C_{\xi_h}\,. \tag{14}$$

The following auxiliary result is the fundamental tool to prove the well-posedness in the case of quadrilaterals.

Lemma 1. *Under the mesh assumptions A.1, A.2, for every $E \in \mathcal{M}_h$ with $N_E = 4$, there exists $C_* > 0$, independent of h_E, such that*

$$\left\|\hat{\Pi}_1^{0,E}\nabla u_h^H\right\|_E \ge C_* \left\|\nabla u_h^H\right\|_E \quad \forall u_h^H \in \mathrm{H}(E)\,. \tag{15}$$

Proof. By definition of $\mathrm{H}(E)$ (11), it is sufficient to prove (15) for $u_h^H = \xi_h$. Using (4) and (5), we get

$$\left\|\hat{\Pi}_1^{0,E}\nabla\xi_h\right\|_E = \sup_{p_2\in\mathbb{P}_2(E)} \frac{\left(\hat{\Pi}_1^{0,E}\nabla\xi_h, \mathbf{curl}\, p_2\right)_E}{\left\|\mathbf{curl}\, p_2\right\|_E} = \sup_{p\in\mathbb{P}_2(E)} \frac{\left(\nabla\xi_h\cdot\boldsymbol{t}^{\partial E}, p_2\right)_{\partial E}}{\left\|\mathbf{curl}\, p_2\right\|_E}\,. \tag{16}$$

For each edge $e_i \in \mathcal{E}_E$, by definition of ξ_h (10) and since the trace of ξ_h is a linear polynomial on each edge of E, we have

$$\nabla\xi_h \cdot \boldsymbol{t}^{e_i} = \frac{2(-1)^{i+1}}{|e_i|}\,. \tag{17}$$

Let M_i, with $i = 1,\dots,4$, be the edge midpoints. Now, we construct $p_2^* \in \mathbb{P}_2(E)$ such that

$$p_2^*(M_i) = (-1)^{i+1}, \quad \forall\, i = 1,\dots,4\,. \tag{18}$$

Notice that by Varignon's theorem, the quadrilateral K_E whose vertices are the edge midpoints $\{M_i\}_{i=1}^4$ is a non degenerate parallelogram (under assumptions A.1 and A.2), whose area is equal to $\frac{|E|}{2}$. Without loss of generality, let us assume $M_4 = (0,0)$, so that $M_2 = M_1 + M_3$, and we define $M_1 = (m_{1x}, m_{1y})$, $M_3 = (m_{3x}, m_{3y})$. Moreover, let $\|M_1\|^2 = m_{1x}^2 + m_{1y}^2$ and $\|M_2\|^2 = m_{2x}^2 + m_{2y}^2$, we can define p_2^* as

$$\begin{aligned} p_2^*(x,y) = {} & -1 + 2\left(\frac{m_{1x}}{\|M_1\|^2} + \frac{m_{2x}}{\|M_2\|^2}\right)x + 2\left(\frac{m_{1y}}{\|M_1\|^2} + \frac{m_{2y}}{\|M_2\|^2}\right)y \\ & -2\left(\frac{m_{1x}m_{2x} - m_{1y}m_{2y}}{\|M_1\|^2\,\|M_2\|^2}\right)(x^2 - y^2) - 4\left(\frac{m_{1x}m_{2y} + m_{1y}m_{2x}}{\|M_1\|^2\,\|M_2\|^2}\right)xy\,. \end{aligned} \tag{19}$$

It is not hard to verify that p_2^* satisfies (18) and that there exists $C_{p^*} > 0$, independent of h_E such that

$$\left\|\mathbf{curl}\, p_2^*\right\|_E = \left\|\nabla p_2^*\right\|_E \le C_{p^*}\,. \tag{20}$$

Finally, starting from (16), and applying Cavalieri–Simpson's quadrature rule, (14), (18) and (20), we have that

$$\begin{aligned} \left\|\hat{\Pi}_1^{0,E}\nabla\xi_h\right\|_E &\ge \frac{\left(\nabla\xi_h\cdot\boldsymbol{t}^{\partial E}, p_2^*\right)_{\partial E}}{\left\|\mathbf{curl}\, p_2^*\right\|_E} = \frac{\sum_{i=1}^4 \frac{(-1)^{i+1}}{3}\left(p_2^*(V_i) + 4p_2^*(M_i) + p_2^*(V_{i+1})\right)}{\left\|\nabla p_2^*\right\|_E} \\ &= \frac{\sum_{i=1}^4 \frac{4(-1)^{i+1}}{3} p_2^*(M_i)}{\left\|\nabla p_2^*\right\|_E} \ge \frac{16}{3C_{p^*}} \ge \frac{16}{3C_{p^*}C_{\xi_h}}\left\|\nabla\xi_h\right\|_E\,, \end{aligned} \tag{21}$$

Thus (15) hold with $C_* = \frac{16}{3C_{p^*}C_{\xi_h}}$. □

Notice that by definition (19), the inf–sup polynomial p_2^* used in the above proof is harmonic. Then, similarly to [16], let $\mathbb{P}_2^H(E) = \mathrm{span}\{x, y, xy, x^2 - y^2\}$ be the space of non-constant harmonic polynomials of degree ≤ 2, when E is a quadrilateral we define the projection operator $\hat{\Pi}_1^{0,E}\nabla : \mathrm{H}^1(E) \to \mathbf{curl}\,\mathbb{P}_2^H(E) \subset \mathbf{curl}\,\mathbb{P}_2(E)$ with $\mathbb{P}_2^H(E)$-orthogonality condition in (4).

Theorem 1. *Under the mesh assumptions A.1, A.2, for every $E \in \mathcal{M}_h$ with $N_E = 4$, the discrete bilinear form a_h^E defined in (6) with $\ell_E = 1$ is coercive, namely there exists $\alpha_*^E > 0$, independent of h_E, such that*

$$a_h^E\left(u_h, u_h\right) \ge \alpha_*^E \left\|\nabla u_h\right\|_E^2 \quad \forall u_h \in \mathcal{V}_{h,1}^E\,. \tag{22}$$

Proof. Let $u_h \in \mathcal{V}_{h,1}^E$ be given. Applying (13), we have the following orthogonal decomposition $u_h = p_1 + u_h^H$, where $p_1 \in \mathbb{P}_1(E)$ and $u_h^H \in \mathrm{H}(E)$, and $\left(\nabla u_h^H, \nabla p_1\right)_E = 0$, that implies $\|\nabla u_h\|_E^2 = \left\|\nabla u_h^H\right\|_E^2 + \|\nabla p_1\|_E^2$. Applying the definition of the projection $\hat{\Pi}_1^{0,E}$ (4), Lemma 1 and noticing $\hat{\Pi}_1^{0,E}\nabla p_1 = \nabla p_1$, we obtain

$$\begin{aligned} a_h^E\left(u_h, u_h\right) &= \left(\hat{\Pi}_1^{0,E}\nabla u_h, \hat{\Pi}_1^{0,E}\nabla u_h\right)_E \\ &= \left(\nabla p_1, \nabla p_1\right)_E + 2\left(\nabla u_h^H, \nabla p_1\right)_E + \left(\hat{\Pi}_1^{0,E}\nabla u_h^H, \hat{\Pi}_1^{0,E}\nabla u_h^H\right)_E \\ &\geq \|\nabla p_1\|_E^2 + C_*^2\left\|\nabla u_h^H\right\|_E^2 \geq \min\{1, C_*\}\|\nabla u_h\|_E^2 , \end{aligned} \tag{23}$$

which yields the thesis, with $\alpha_*^E := \min\{1, C_*\}$. □

4.2. Local coercivity for $N_E \geq 5$

In this section we deal with the case $N_E \geq 5$. This proof requires the following assumption on ℓ_E.

H.1 ℓ_E is such that there exists a set of degrees of freedom for $p \in \mathbb{P}_{\ell_E+1}(E)$ which contains the integral mean $\frac{1}{|e|}\int_e p$ on each edge $e \in \mathcal{E}_E$.

Theorem 2. *Under assumptions A.1, A.2 and H.1, for every $E \in \mathcal{M}_h$, the discrete bilinear form a_h^E defined by (6) is coercive, namely there exists $\alpha_*^E > 0$, independent of h_E, such that*

$$a_h^E\left(u_h, u_h\right) \geq \alpha_*^E\|\nabla u_h\|_E^2 \quad \forall u_h \in \mathcal{V}_{h,1}^E . \tag{24}$$

Proof. $\forall E \in \mathcal{M}_h$, $\forall n \in \mathbb{N}$ we define the auxiliary space:

$$\mathbb{P}^0_{\ell_E+1}(E) = \left\{ p \in \mathbb{P}_{\ell_E+1}(E) : \int_{\partial E} p = 0 \right\}.$$

Using the definition of the norm of the operator $\hat{\Pi}_{\ell_E}^{0,E}$, (4) and (5), we get, $\forall u_h \in \mathcal{V}_{h,1}^E$,

$$\left\|\hat{\Pi}_{\ell_E}^{0,E}\nabla u_h\right\|_E = \sup_{p\in\mathbb{P}^0_{\ell_E+1}(E)} \frac{\left(\hat{\Pi}_{\ell_E}^{0,E}\nabla u_h, \mathbf{curl}\, p\right)_E}{\|\mathbf{curl}\, p\|_E} = \sup_{p\in\mathbb{P}^0_{\ell_E+1}(E)} \frac{\left(\nabla u_h \cdot \boldsymbol{t}^{\partial E}, p\right)_{\partial E}}{\|\mathbf{curl}\, p\|_E} . \tag{25}$$

Denoting by $\{\phi\}_{i=1}^{N_E}$ the set of Lagrangian basis functions of $\mathcal{V}_{h,1}^E$, we have that $u_h = \sum_{i=1}^{N_E} c_i\phi_i$ and for each edge $e_i \in \mathcal{E}_E$

$$\nabla u_h \cdot \boldsymbol{t}^{e_i} = \frac{c_{i+1} - c_i}{|e_i|} , \tag{26}$$

Moreover, let $\delta_i := c_{i+1} - c_i$. For each $p \in \mathbb{P}^0_{\ell_E+1}(E)$ we get

$$\left(\nabla u_h \cdot \boldsymbol{t}^{\partial E}, p\right)_{\partial E} = \sum_{i=1}^{N_E} \frac{\delta_i}{|e_i|}\int_{e_i} p . \tag{27}$$

Under assumption H.1 we can define $\tilde{p} \in \mathbb{P}^0_{\ell_E+1}(E)$ such that its degrees of freedom are

$$\frac{1}{|e_i|}\int_{e_i}\tilde{p} = \frac{h_E}{|e_i|}\delta_i \quad \forall i = 1, \dots, N_E,$$

and all other degrees of freedom of $\tilde{p}$ are zero. Since $\sum_{i=1}^{N_E}\delta_i = 0$, then $\int_{\partial E}\tilde{p} = h_E\sum_{i=1}^{N_E}\delta_i = 0$ and, applying the equivalence of norms between $\|\nabla\tilde{p}\|_E$ and the l^2-norm of the vector of degrees of freedom of $\tilde{p}$, $\exists C_p > 0$ independent of h_E such that

$$\|\mathbf{curl}\,\tilde{p}\|_E^2 = \|\nabla\tilde{p}\|_E^2 \leq C_p^2\sum_{i=1}^{N_E}\left(\frac{1}{|e_i|}\int_{e_i}\tilde{p}\right)^2 \leq \frac{C_p^2}{\kappa}\sum_{i=1}^{N_E}\frac{h_E}{|e_i|}\delta_i^2 = \frac{C_p^2}{\kappa}|u_h|_{\partial E}^2 , \tag{28}$$

where we define $|u_h|_{\partial E} := \left(h_E\sum_{i=1}^{N_E}\|\nabla u_h \cdot \boldsymbol{t}^{e_i}\|_{e_i}^2\right)^{\frac{1}{2}} = \left(\sum_{i=1}^{N_E}\frac{h_E}{|e_i|}\delta_i^2\right)^{\frac{1}{2}}$. It was proved in [2,21] that, considering $u_h \in \mathcal{V}_{h,1}^E$ such that $\int_{\partial E} u_h = 0$ then $|u_h|_{\partial E}$ is a norm for u_h,

$$|u_h|_{\partial E} \geq C_u\|\nabla u_h\|_E , \tag{29}$$

holds true with a constant C_u only depending on the radius ρ of the mesh assumption **A.1**. With the above definition of $\tilde{p}$ and applying (28), and (29), starting from (25) we get,

$$\begin{aligned}\left\|\hat{\Pi}^{0,E}_{\ell_E}\nabla u_h\right\|_E &= \sup_{p\in\mathbb{P}^0_{\ell_E+1}(E)} \frac{\left(\nabla u_h\cdot \boldsymbol{t}^{\partial E}, p\right)_{\partial E}}{\|\mathbf{curl}\, p\|_E} \geq \frac{\sum_{i=1}^{N_E}\delta_i \frac{1}{|e_i|}\int_{e_i}\tilde{p}}{\|\mathbf{curl}\,\tilde{p}\|_E} \\ &= \frac{\sum_{i=1}^{N_E}\delta_i^2\frac{h_E}{|e_i|}}{\|\mathbf{curl}\,\tilde{p}\|_E} \geq \frac{\sqrt{\kappa}\,|u_h|^2_{\partial E}}{C_p\,|u_h|_{\partial E}} \geq \frac{\sqrt{\kappa}C_u}{C_p}\left\|\nabla u_h\right\|_E .\end{aligned} \tag{30}$$

Then, (24) is proved. □

In Appendix we provide some theoretical results about the validity of Assumption **H.1** for certain classes of polygons. The following theorem summarizes those results.

Theorem 3. *Let $E\in\mathcal{M}_h$ be such that $N_E\geq 5$. Then the following results hold true.*

- *If E is strictly convex, then Assumption **H.1** is satisfied by $\ell_E = N_E - 3$.*
- *If E has one reentrant corner and such that at least one edge lies on the boundary of the kernel of the polygon, then, Assumption **H.1** is satisfied by $\ell_E = N_E - 3$. This also holds if E has two aligned edges.*
- *If E is a polygon with aligned edges such that the edges lie on exactly three straight lines, then Assumption **H.1** is satisfied by $\ell_E = N_E - 4$.*

Notice that the case of convex polygons is a direct consequence of a known result about mean value interpolation (see [26, Theorem 12.1 and Definition 9.9]).

In Section 7 we provide an algorithm for the numerical computation of ℓ_E ensuring coercivity. In general, the computed ℓ_E results to be smaller than the ones that guarantee coercivity by the above theorem.

4.3. Global coercivity

Now, we state the coercivity of the global bilinear form a_h defined in (7) with respect to the standard $\mathrm{H}^1_0(\Omega)$ norm.

Theorem 4. *For each $E\in\mathcal{M}_h$ we assume that*

- *if $N_E = 3$, $\ell_E = 0$,*
- *if $N_E = 4$, $\ell_E = 1$ and the local projection operator $\hat{\Pi}^{0,E}_1\nabla$ is defined onto the space of* **curl** *of quadratic harmonic polynomials,*
- *if $N_E\geq 5$, **H.1** is satisfied.*

Then, $\exists C_*$ independent of h such that

$$a_h\left(v_h, v_h\right) \geq C_*\left\|\nabla v_h\right\|^2_\Omega \quad \forall v_h\in\mathcal{V}_{h,1} . \tag{31}$$

Proof. Applying the definition of a_h and local coercivity Theorems 1 and 2, we have

$$a_h\left(v_h, v_h\right) = \sum_{E\in\mathcal{M}_h} a^E_h\left(v_h, v_h\right) \geq \sum_{E\in\mathcal{M}_h}\alpha^E_*\left\|\nabla v_h\right\|^2_E \geq C_*\left\|\nabla v_h\right\|^2_\Omega , \tag{32}$$

where $C_* := \min_{E\in\mathcal{M}_h} C(E)$. □

This theorem and the global continuity of a_h, which follows from Proposition 1, imply that a_h satisfies the hypothesis of the Lax–Milgram theorem, hence the discrete problem (8) admits a unique solution.

5. A priori error analysis

The proof of a priori error estimates for problem (8) is obtained following the same analysis done in [15]. First, we recall some auxiliary results that are well-known in the literature about polynomial approximation.

Lemma 2. *Under the current mesh assumptions, $\forall E\in\mathcal{M}_h$, if $u\in\mathrm{H}^1(E)$ then $\exists C>0$ independent of h_E such that*

$$\left\|u - \Pi^{0,E}_0 u\right\|_E \leq C h_E\left\|\nabla u\right\|_E . \tag{33}$$

Moreover if $u\in\mathrm{H}^2(E)$ then $\exists C>0$ independent of h_E such that

$$\left\|\nabla u - \Pi^{0,E}_0\nabla u\right\|_E \leq C h_E\left|u\right|_2 . \tag{34}$$

Furthermore, we recall the following interpolation estimate, that was proved in [27].

Lemma 3. *Under the current mesh assumptions, $\forall E \in \mathcal{M}_h$, if $u \in \mathrm{H}^2(E)$ then there exists $u_I \in \mathcal{V}_{h,1}^E$ such that*

$$\|u - u_I\|_E + h_E \|\nabla u - \nabla u_I\|_E \leq C h_E^2 |u|_2 , \tag{35}$$

with a constant C independent of h_E.

The above theoretical tools are used to prove the following a priori error estimate.

Theorem 5. *Let $u \in \mathrm{H}^2(\Omega)$ be the exact solution to (2) and let $u_h \in \mathcal{V}_{h,1}^E$ be the solution to the discrete problem (8), with ℓ_E chosen locally $\forall E \in \mathcal{M}_h$ according to Sections 4.1 and 4.2. Then, under the current mesh regularity assumptions,*

$$\|\nabla u - \nabla u_h\| \leq C h \left(|u|_2 + \sum_{E \in \mathcal{M}_h} \left\| f - \Pi_0^{0,E} f \right\| \right) , \tag{36}$$

with a constant C independent of the mesh-size.

Proof. Exploiting Lemma 3, there exists $u_I \in \mathcal{V}_{h,1}$ such that

$$\|\nabla u - \nabla u_h\| \leq \|\nabla u - \nabla u_I\| + \|\nabla u_I - \nabla u_h\| \leq C h |u|_2 + \|\nabla u_I - \nabla u_h\| .$$

Then, let $e_h = u_I - u_h \in \mathcal{V}_{h,1}$. Since ℓ_E is chosen in order to provide well-posedness, exploiting problems (8) and (2) we get

$$\begin{aligned} \|\nabla u_I - \nabla u_h\|^2 &\leq \frac{1}{\alpha_*} \sum_{E \in \mathcal{M}_h} a_h^E \left(u_I - u_h, e_h \right) \\ &= \frac{1}{\alpha_*} \sum_{E \in \mathcal{M}_h} a_h^E \left(u_I - u, e_h \right) + a_h^E \left(u, e_h \right) - \left(\nabla u, \nabla e_h \right)_E + \left(f, e_h - \Pi_0^{0,E} e_h \right)_E . \end{aligned}$$

The first local term is estimated using the continuity of a_h^E (9) and the interpolation estimate (35):

$$a_h^E \left(u_I - u, e_h \right) \leq \|\nabla u_I - \nabla u\|_E \|\nabla e_h\|_E \leq C h_E \|\nabla e_h\|_E |u|_{2,E} .$$

Regarding the second and third local terms, they provide the approximation error with respect to polynomials and can be bound exploiting the definition of $\hat{\Pi}_{\ell_E}^{0,E}$ (4), and a Cauchy–Schwarz inequality as follows:

$$a_h^E \left(u, e_h \right) - \left(\nabla u, \nabla e_h \right)_E = \left(\hat{\Pi}_{\ell_E}^{0,E} \nabla u - \nabla u, \nabla e_h \right)_E \leq \left\| \hat{\Pi}_{\ell_E}^{0,E} \nabla u - \nabla u \right\|_E \|\nabla e_h\|_E ,$$

and the above projection error, since $\left[\mathbb{P}_0(E) \right]^2 \subseteq \mathbf{curl}\, \mathbb{P}_{\ell_E+1}(E)$ $\forall \ell_E \geq 0$, can be bound exploiting (34):

$$\left\| \hat{\Pi}_{\ell_E}^{0,E} \nabla u - \nabla u \right\|_E = \inf_{\boldsymbol{p} \in \mathbf{curl}\, \mathbb{P}_{\ell_E+1}(E)} \|\boldsymbol{p} - \nabla u\|_E \leq \left\| \Pi_0^{0,E} \nabla u - \nabla u \right\|_E \leq C h_E |u|_2 .$$

Finally, the term involving the right-hand side can be bound exploiting the definition of $\Pi_0^{0,E}$ and the projection estimate (33):

$$\begin{aligned} \left(f, e_h - \Pi_0^{0,E} e_h \right)_E &= \left(f - \Pi_0^{0,E} f, e_h - \Pi_0^{0,E} e_h \right)_E \\ &\leq \left\| f - \Pi_0^{0,E} f \right\|_E \left\| e_h - \Pi_0^{0,E} e_h \right\|_E \leq C h_E \left\| f - \Pi_0^{0,E} f \right\|_E \|\nabla e_h\|_E . \end{aligned}$$

Collecting the above estimates, we obtain (36) □

Following the same proof as in [15, Theorem 5.2] and exploiting estimate (36), we can also obtain the following a priori estimate in the L^2-norm.

Theorem 6. *Let u be the exact solution to (2) and let $u_h \in \mathcal{V}_{h,1}^E$ be the solution to the discrete problem (8), with ℓ_E chosen locally $\forall E \in \mathcal{M}_h$ according to Sections 4.1 and 4.2. Then, under the current mesh regularity assumptions if $u \in \mathrm{H}^2(\Omega)$ then, assuming $f \in \mathrm{H}^1(E)$ $\forall E \in \mathcal{M}_h$,*

$$\|u - u_h\| \leq C h^2 \left(|u|_2 + \sum_{E \in \mathcal{M}_h} \|\nabla f\|_E \right) , \tag{37}$$

Remark 2. The local regularity of the right-hand side required in Theorem 6 can be relaxed if we discretize the right-hand side with a projection of test functions on $\mathbb{P}_1(E)$. In that case, with $f \in \mathrm{L}^2(\Omega)$ we get

$$\|u - u_h\|_E \leq C h^2 \left(|u|_2 + \sum_{E \in \mathcal{M}_h} \left\| f - \Pi_1^{0,E} f \right\|_E \right) .$$

Remark 3 (*Extension to more general elliptic problems*). Consider a uniformly elliptic tensor $\mathcal{K} \in \mathrm{L}^\infty(\Omega)$, a scalar function $\gamma \in \mathrm{L}^\infty(\Omega)$ and the following model problem:

$$\begin{cases} -\nabla \cdot (\mathcal{K}\nabla u) + \gamma u = f & \text{in } \Omega, \\ u = 0 & \text{on } \partial\Omega. \end{cases} \tag{38}$$

The coercivity of the bilinear form defined by (6) and (7) allows the discretization: find $u_h \in \mathcal{V}_{h,1}$ such that

$$\sum_{E\in\mathcal{M}_h} \left(\mathcal{K}\hat{\Pi}^{0,E}_{\ell_E}\nabla u_h, \hat{\Pi}^{0,E}_{\ell_E}\nabla v_h\right)_E + \left(\gamma \Pi^{0,E}_0 u_h, \Pi^{0,E}_0 v_h\right)_E = \sum_{E\in\mathcal{M}_h} \left(f, \Pi^{0,E}_0 v_h\right)_E \tag{39}$$

for each $v_h \in \mathcal{V}_{h,1}$. Indeed, if the local projection operators are coercive on each polygon, we can prove the well-posedness of (39), exploiting the ellipticity of $\mathcal{K}$ and following [15, Lemma 5.7]. Optimal order a priori error estimates can be proved proceeding as in Theorem 5 and [15, Theorem 5.1 and 5.2].

6. Computation of $\hat{\Pi}^{0,E}_{\ell_E}\nabla$

Algorithm 1 Algorithm for the computation of ℓ_E on a given polygon

Input: A polygon $E \in \mathcal{M}_h$ with $N_E \geq 5$
Let ℓ_E be the smallest number satisfying (41)
Compute the matrix B such that $B_{ij} = \left(\frac{\partial\varphi_j}{\partial t}, p_i\right)_{\partial E}$ $\forall p_i$ basis of $\mathbb{P}_{\ell_E+1}(E)$
Perform a QR decomposition of $B^\intercal$: $B^\intercal = QR$
$N \leftarrow$ number of diagonal elements of R whose absolute value is $\geq$ 1e − 12
while $N < N_E - 1$ **do**
  $\ell_E \leftarrow \ell_E + 1$
  Compute $\tilde{B}$ such that $\tilde{B}_{ij} = \left(\frac{\partial\varphi_j}{\partial t}, \tilde{p}_i\right)_{\partial E}$ $\forall \tilde{p}_i$ basis of $\mathbb{P}_{\ell_E+1}(E)/\mathbb{P}_{\ell_E}(E)$
  Perform a QR decomposition of the matrix $\tilde{B}^\intercal - QQ^\intercal\tilde{B}^\intercal = \tilde{Q}\tilde{R}$
  $B^\intercal \leftarrow \begin{bmatrix} B^\intercal & \tilde{B}^\intercal \end{bmatrix}$
  $R \leftarrow \begin{bmatrix} R & Q^\intercal\tilde{B}^\intercal \\ 0 & \tilde{R} \end{bmatrix}$
  $Q \leftarrow \begin{bmatrix} Q & \tilde{Q} \end{bmatrix}$
  $N \leftarrow$ number of diagonal elements of R whose absolute value is $\geq$ 1e − 12
end while
return ℓ_E, B

Let us describe the construction of $\hat{\Pi}^{0,E}_{\ell_E}\nabla$ on a generic polygon $E \in \mathcal{M}_h$. The computation of the matrix representing the gradient projection follows standard VEM practice (see [24]). We recall it here for the sake of clarity of exposition. In the case $N_E = 4$ we use curls of harmonic polynomials of degree 2, while in other cases we use curls of generic polynomials. In general, given a polynomial space $\mathcal{P}(E)$, let $\hat{\Pi}^{0,E}_{\ell_E}\nabla : \mathcal{V}^E_{h,1} \to \mathbf{curl}\,\mathcal{P}(E)$ be such that

$$\forall\varphi \in \mathcal{V}^E_{h,1}, \left(\hat{\Pi}^{0,E}_{\ell_E}\nabla\varphi - \nabla\varphi, \mathbf{curl}\, p\right)_E = 0 \quad \forall p \in \mathcal{P}(E).$$

Let $\{\varphi_j, \quad j = 1, \dots, N_E\}$ be a basis of $\mathcal{V}^E_{h,1}$ and consider a basis $\{m_k, \quad k = 1, \dots, \dim\mathcal{P}(E) - 1\}$ of $\mathcal{P}(E)/\mathbb{P}_0(E)$. Since $\hat{\Pi}^{0,E}_{\ell_E}\nabla\varphi_j \in \mathbf{curl}\,\mathcal{P}(E)$, we have

$$\hat{\Pi}^{0,E}_{\ell_E}\nabla\varphi_j = \sum_{k=1}^{\dim\mathcal{P}(E)-1} \pi_{kj}\mathbf{curl}\, m_k.$$

It is then easy to check that the matrix $\hat{\Pi}$ collecting the coefficients π_{kj} is obtained by solving the matrix system

$$G\hat{\Pi} = B, \tag{40}$$

where $G_{ik} = \left(\mathbf{curl}\, m_i, \mathbf{curl}\, m_k\right)_E = \left(\nabla m_i, \nabla m_k\right)_E$ is symmetric and positive definite and $B_{ij} = \left(\nabla\varphi_j \cdot \mathbf{t}, m_i\right)_{\partial E}$.

If $N_E = 4$, we set $\mathcal{P}(E) = \{p \in \mathbb{P}_2(E) : \Delta p = 0\}$ and solve (40). Notice that in this case the computation of G can be performed by computing boundary integrals, indeed in this case $\left(\nabla m_i, \nabla m_k\right)_E = \left(m_i, \frac{\partial m_k}{\partial n}\right)_{\partial E}$.

If $N_E \geq 5$, we implement the following algorithm designed to numerically enforcing coercivity. Given a polygon $E \in \mathcal{M}_h$ and a degree ℓ_E, let $\{m_i, \quad i = 1, \dots, \frac{1}{2}(\ell_E + 2)(\ell_E + 3) - 1\}$ be a set of basis functions of $\mathbb{P}_{\ell_E+1}(E)/\mathbb{P}_0(E)$. Since $\dim\mathcal{V}^E_{h,1} = N_E$, and thus $\dim\nabla\mathcal{V}^E_{h,1} = N_E - 1$, then $\hat{\Pi}^{0,E}_{\ell_E} : \nabla\mathcal{V}^E_{h,1} \to \mathbf{curl}\,\mathbb{P}_{\ell_E+1}(E)$ is injective if and only if the dimension of its range is $N_E - 1$. This implies that the desired rank of $\hat{\Pi}$ is $N_E - 1$ and, since G is non-singular, this is guaranteed if the rank of B is also $N_E - 1$. In order to

Table 1
Convex polygons. Values of ℓ_E provided by Algorithm 1 and corresponding σ_{N_E-1}. The asterisk denotes the use of curls of harmonic polynomials of degree 2 (see Lemma 1).

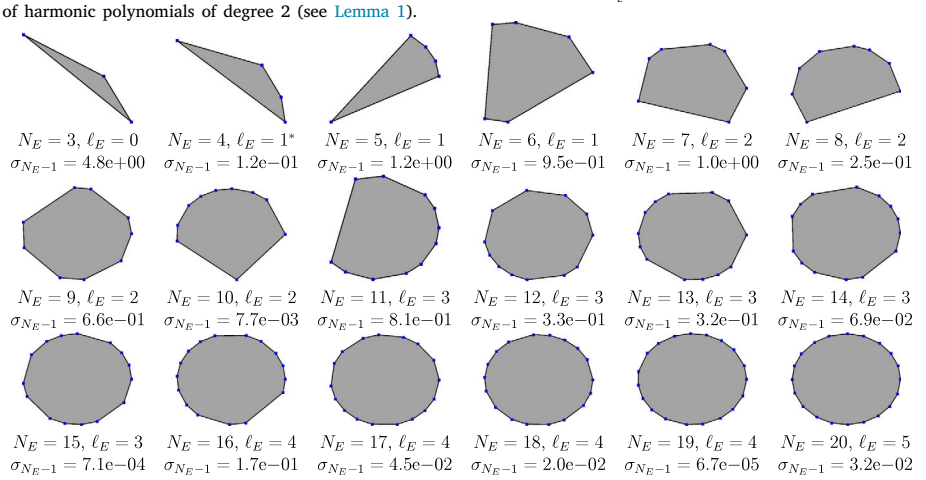

determine for each polygon E the minimum ℓ_E providing numerically the coercivity, we apply Algorithm 1. We first set ℓ_E equal to the necessary condition of the injectivity for the projector $\hat{\Pi}^{0,E}_{\ell_E} : \nabla \mathcal{V}^E_{h,1} \to \mathbf{curl}\, \mathbb{P}_{\ell_E+1}(E)$, i.e.

$$\begin{aligned} &\dim \mathbf{curl}\, \mathbb{P}_{\ell_E+1}(E) = \dim \mathbb{P}_{\ell_E+1}(E) - 1 \geq \dim \nabla \mathcal{V}^E_{h,1} = \dim \mathcal{V}^E_{h,1} - 1 \\ &\quad \iff (\ell_E + 2)(\ell_E + 3) \geq 2N_E\,. \end{aligned} \tag{41}$$

Then, we start by computing the corresponding matrix B, we perform its QR decomposition and we evaluate if the number of non-zero elements of the diagonal of the matrix R is equal to the dimension of the space of gradients of VEM functions, i.e. $N_E - 1$. If not, we increase ℓ_E until we satisfy the condition. Notice that the QR decomposition is updated at each iteration and that the algorithm is based on the computation of boundary integrals only. Once we have the value of ℓ_E and the corresponding matrix B, we compute the matrix G and solve (40). Note that the additional cost of performing Algorithm 1 with respect to knowing ℓ_E in advance is the QR decomposition of a matrix of dimension $\dim \mathbb{P}_{\ell_E+1}(E) \times N_E$. In the numerical tests, we consider the set of basis functions of the space $\mathbb{P}_{\ell_E+1}(E) \setminus \mathbb{P}_0(E)$ defined as follows:

$$\mathcal{M}_{\ell_E+1}(E) = \left\{ m \in \mathbb{P}_{\ell_E+1}(E) : m(x,y) = \frac{(x - x_E)^{\alpha_1}(y - y_E)^{\alpha_2}}{h_E}, \right.$$
$$\left. \forall \alpha_1, \alpha_2 > 0 \text{ such that } 1 \leq \alpha_1 + \alpha_2 \leq \ell_E + 1 \right\}.$$

Remark 4. Notice that the elements of B are invariant with respect to rescaling of the polygon, and the same holds for $\|\mathbf{curl}\, p\|_E$, $\forall p \in \mathcal{P}(E)/\mathbb{P}_0(E)$. This implies that the smallest non zero singular value of B is independent of h_E, and thus it holds true that, $\forall \varphi_i$,

$$\left\| \hat{\Pi}^{0,E}_{\ell_E} \nabla \varphi_i \right\|_E = \sup_{p \in \mathbb{P}_{\ell_E+1}(E)} \frac{\left(\nabla \varphi_i \cdot \boldsymbol{t}^{\partial E}, p\right)_{\partial E}}{\|\mathbf{curl}\, p\|_E} \geq \alpha_* \left\| \nabla \varphi_i \right\|_E , \tag{42}$$

with α_* independent of h_E.

7. Numerical results

Here, we first consider single polygons and investigate numerically which is the minimum degree ℓ_E providing coercivity, then we carry out some convergence tests.

7.1. Coercivity tests

In this section, we consider different sets of polygons and we investigate numerically the minimum ℓ_E chosen by Algorithm 1 comparing it with the ℓ_E given by the necessary condition (41) and, if available, with the sufficient condition theoretically proved in Appendix. To test numerically the coercivity of the bilinear form a^E_h, for each polygon we compute the $(N_E - 1)$th from largest to smallest singular value of the local stiffness matrix $A^E \in \mathbb{R}^{N_E, N_E}$, denoted by σ_{N_E-1}, using the value of ℓ_E provided by Algorithm 1; $\sigma_{N_E-1} \neq 0$ ensures the rank of the stiffness matrix be equal to $N_E - 1$.

We consider five sets of polygons chosen in order to highlight different geometrical features that can influence the choice of the local polynomial projection degree.

Table 2
Regular polygons. Values of ℓ_E provided by Algorithm 1 and corresponding σ_{N_E-1}.

N_E	3	4	5	6	7	8	9	10	11
ℓ_E	0	1[a]	1	2	2	3	3	4	4
σ_{N_E-1}	8.2e−01	3.3e−01	6.3e−01	5.8e−01	5.3e−01	5.0e−01	4.7e−01	4.5e−01	4.3e−01
N_E	12	13	14	15	16	17	18	19	20
ℓ_E	5	5	6	6	7	7	8	8	9
σ_{N_E-1}	4.1e−01	3.9e−01	3.8e−01	3.7e−01	3.5e−01	3.4e−01	3.3e−01	3.2e−01	3.2e−01

[a] Denotes the use of curls of harmonic polynomials of degree 2 (see Lemma 1).

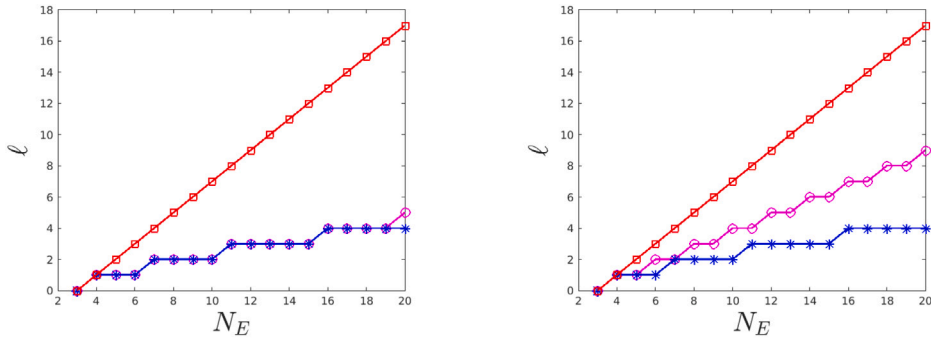

(a) *Convex Polygons* (b) *Regular Polygons*

Fig. 1. Comparison between the ℓ_E provided by Algorithm 1 (pink line) and the ones relative to theoretical results, that is $\ell_E = N_E - 3$, provided by Theorem 3 (red line) and the necessary condition on ℓ_E, satisfying (41) (blue line). (For interpretation of the references to colour in this figure legend, the reader is referred to the web version of this article.)

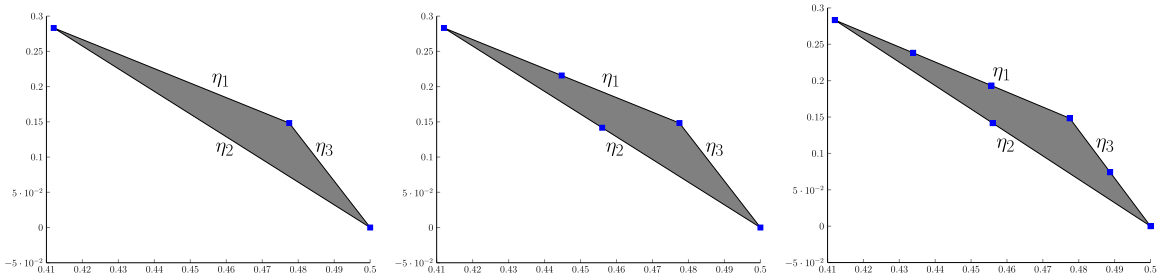

(a) Starting triangle. $\alpha_1 = 1$, $\alpha_2 = 1$, $\alpha_3 = 1$ (b) $\alpha_1 = 2$, $\alpha_2 = 2$, $\alpha_3 = 1$ (c) $\alpha_1 = 3$, $\alpha_2 = 2$, $\alpha_3 = 2$

Fig. 2. Examples of "triangular" polygons.

7.1.1. Convex polygons

First, we consider two family of convex polygons. Table 1 refers to a sequence of generic convex polygons, displayed in the table. Table 2 we consider regular convex polygons, defined by the vertices $V_i = (\cos(\beta_i), \sin(\beta_i))$, with $\beta_i = \frac{(i-1)\pi}{N_E}$ $i = 1, \dots N_E$. In Table 1 we can see that the computed singular values σ_{N_E-1} are significantly larger than machine precision. Concerning Table 2, we can see that the polynomial degree provided by the algorithm corresponds to the one that we obtain if we use harmonic polynomials only (see [14]). We notice that, in the case of regular polygons, the scheme is stable if and only if the projection space contains the curls of harmonic polynomials of degree at least $\ell_E + 1 = \frac{N_E-3}{2} + 1$, i.e. with the choice $2\ell_E \geq N_E - 3$.

From Fig. 1, we can observe that the projection degree computed numerically is much smaller than the one provided by Theorem 3.

7.1.2. Polygons with edges on three straight lines

The third test that we consider relates to the third point of Theorem 3 (whose proof is given by Proposition 4 in Appendix). We consider polygons whose boundary can be described by three straight lines, that in the following are called, for the sake of brevity, "triangular polygons". Following the notation of Proposition 4, let α_i $(i = 1, 2, 3)$ denote the number of aligned edges of the polygon on each edge η_i of the underlying triangle. We consider polygons obtained starting from a triangle creating α_i aligned edges of the same length on each η_i. Each polygon in this sequence is identified by the triplet $(\alpha_1, \alpha_2, \alpha_3)$. Fig. 2 depicts the starting triangle and

Table 3
"Triangular" polygons. Values of ℓ_E provided by Algorithm 1 and corresponding σ_{N_E-1}.

N_E	5	5	6	6	6
$(\alpha_1, \alpha_2, \alpha_3)$	(2,2,1)	(3,1,1)	(2,2,2)	(3,2,1)	(4,1,1)
ℓ_E	1	1	2	1	2
σ_{N_E-1}	4.4e+00	4.4e+00	4.3e+00	4.2e+00	4.3e+00
N_E	7	7	7	7	
$(\alpha_1, \alpha_2, \alpha_3)$	(5,1,1)	(4,2,1)	(3,2,2)	(3,3,1)	
ℓ_E	3	2	2	2	
σ_{N_E-1}	4.1e+00	4.0e+00	4.0e+00	4.0e+00	

Table 4
Concave polygons. Values of ℓ_E provided by Algorithm 1 and corresponding σ_{N_E-1}. The asterisk denotes the use of curls of harmonic polynomials of degree 2 (see Lemma 1). The second polygon of the table was suggested by Professor A. Russo.

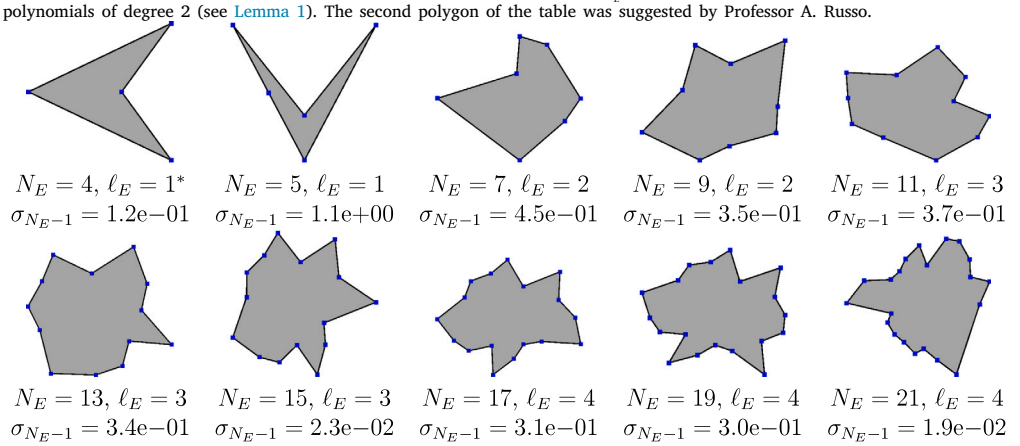

Table 5
Regular stars. Values of ℓ_E provided by Algorithm 1 and corresponding σ_{N_E-1}.

N_E	6	8	10	12	14	16	18	20
ℓ_E	2	3	4	5	6	7	8	9
σ_{N_E-1}	5.1e−01	4.5e−01	4.0e−01	3.7e−01	3.4e−01	3.2e−01	3.0e−01	2.8e−01

some polygons of the sequence. Table 3 shows the computed σ_{N_E-1}, corresponding to the ℓ_E provided by Algorithm 1, which are all $O(1)$.

7.1.3. Concave polygons and regular stars

In Table 4 for non-regular concave polygons, we report the values ℓ_E provided by Algorithm 1 and the computed σ_{N_E-1}, all well-detached from zero. Finally, we consider a sequence of regular stars. The $2n$ vertices of these stars are defined for $i = 1, \dots, n$ by

$$V_{2i-1} = \rho_{\max} \begin{pmatrix} \cos\left(\frac{(2i-2)\pi}{n}\right) \\ \sin\left(\frac{(2i-2)\pi}{n}\right) \end{pmatrix}, \quad V_{2i} = \rho_{\min} \begin{pmatrix} \cos\left(\frac{(2i-1)\pi}{n}\right) \\ \sin\left(\frac{(2i-1)\pi}{n}\right) \end{pmatrix}$$

and we choose $\rho_{\max} = 1.5$ and $\rho_{\min} = 0.5$. Table 5 displays the values ℓ_E provided by Algorithm 1, for which we notice that the value ℓ_E corresponds to having in the polynomial basis a number of harmonic polynomials of degree $\ell_E + 1$ with $\ell_E \geq \frac{N_E-3}{2}$. Also in this case, the computed σ_{N_E-1} are well-detached from zero.

Fig. 3 displays the ℓ_E computed by Algorithm 1 and the ℓ_E corresponding to the necessary condition (41). Also in this case the comment provided for Fig. 1 holds true.

7.2. Convergence tests

Let us consider problem (1) on the unit square with homogeneous Dirichlet boundary conditions and the right-hand side defined such that the exact solution is

$$u(x, y) = 16xy(1 - x)(1 - y).$$

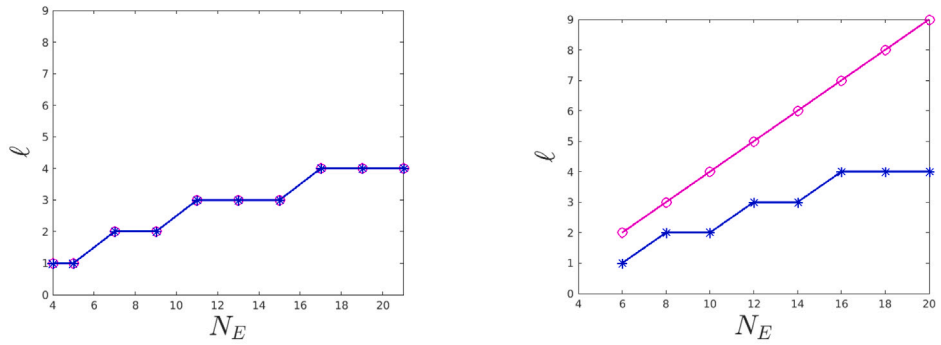

(a) *Non Convex Polygons* (b) *Regular Stars*

Fig. 3. Comparison between the sufficient ℓ_E obtained numerical and the one relative to theoretical results. Pink: computed ℓ_E. Blue: necessary condition on ℓ_E (satisfying (41)). (For interpretation of the references to colour in this figure legend, the reader is referred to the web version of this article.)

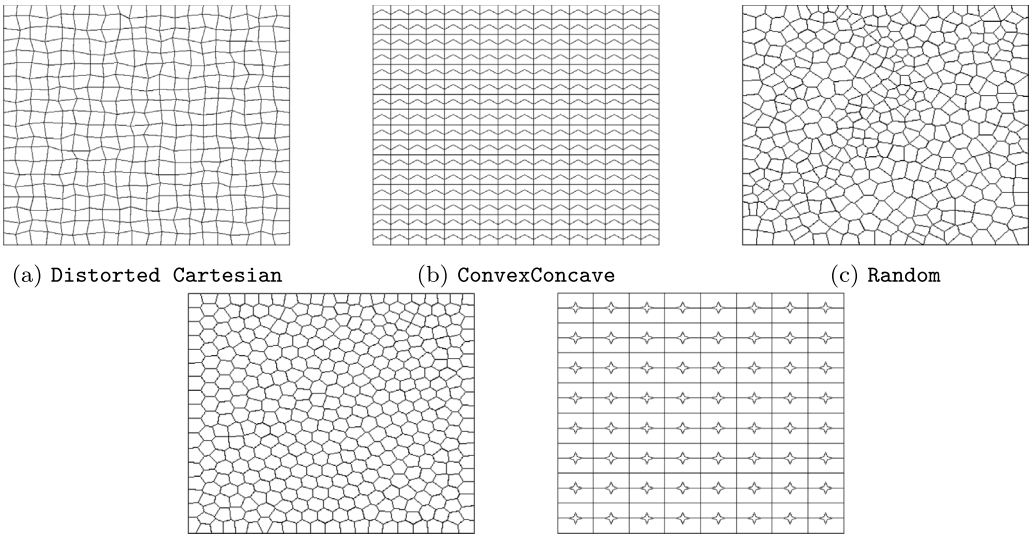

(a) `Distorted Cartesian` (b) `ConvexConcave` (c) `Random`

(d) `Polymesher` (e) `Star`

Fig. 4. Meshes used for convergence tests.

In the following, we show, the convergence curves of the L^2 and H^1 errors that we measure as follows,

$$L^2 \text{ error } = \frac{1}{\|u\|}\sqrt{\sum_{E\in\mathcal{M}_h}\left\|\Pi_1^{\nabla,E}u_h - u\right\|_E^2},$$

$$H^1 \text{ error } = \frac{1}{\|\nabla u\|}\sqrt{\sum_{E\in\mathcal{M}_h}\left\|\nabla\Pi_1^{\nabla,E}u_h - \nabla u\right\|_E^2},$$

where u_h is the discrete solution of (8), obtained selecting locally ℓ_E as described in the previous section. We also solve the test problem with the standard VEM method [15], where

$$a_h^E\left(u_h, v_h\right) = \left(\Pi_0^{0,E}\nabla u_h, \Pi_0^{0,E}\nabla v_h\right)_E + S^E\left((I-\Pi_1^{\nabla,E})u_h, (I-\Pi_1^{\nabla,E})v_h\right) \tag{43}$$

and $S^E : \mathcal{V}_{h,1}^E \times \mathcal{V}_{h,1}^E \to \mathbb{R}$ denotes the local *dofi-dofi* stabilizing bilinear form

$$S^E\left(u_h, v_h\right) = \chi^E(u_h)\cdot\chi^E(v_h) \quad \forall u_h, v_h \in \mathcal{V}_{h,1}^E,$$

with $\chi^E(v_h)$ defined as the vector of degrees of freedom of v_h on E. We consider five sequences of meshes for the convergence test. The first sequence, labeled `DistortedCartesian`, is a tessellation made by quadrilaterals, obtained perturbing a cartesian mesh, as shown in Fig. 4(a). The second sequence, shown in Fig. 4(b) and labeled `ConvexConcave`, is made by pentagons, half of which are concave. Then, the third and the fourth sequences, depicted in Figs. 4(c) and 4(d), labeled `Random` and `Polymesher`

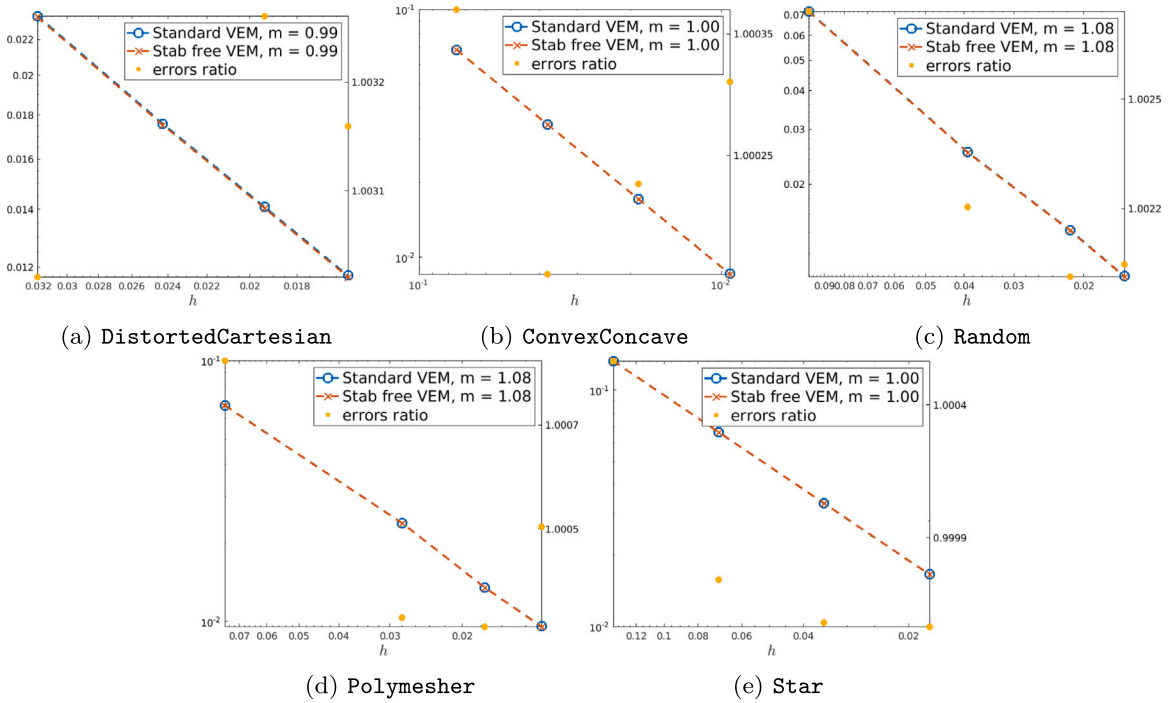

Fig. 5. Tests on Poisson problem: H^1 convergence plots.

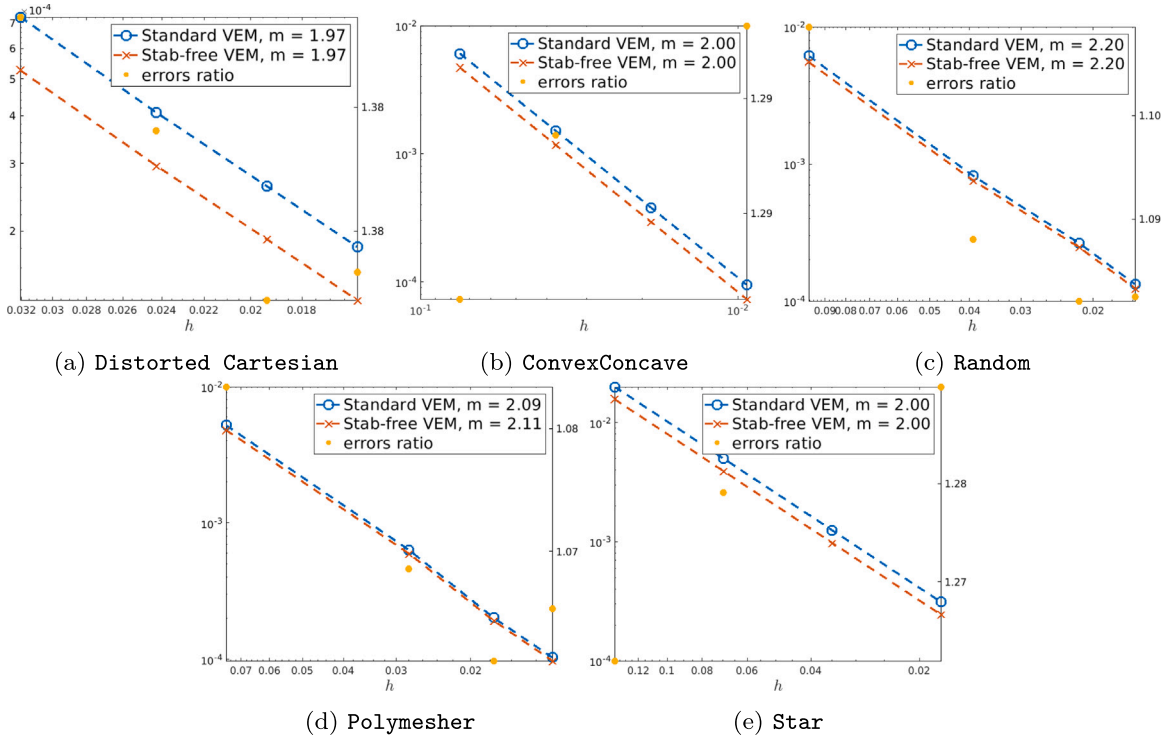

Fig. 6. Tests on Poisson problem: L^2 convergence plots.

respectively, are made by convex polygons and are obtained using *Polymesher* [28], with two different smoothing parameters. Finally, the last sequence, labeled `Star`, is a non-convex tessellation made by octagons and nonagons, shown in Fig. 4(e). For the five mesh

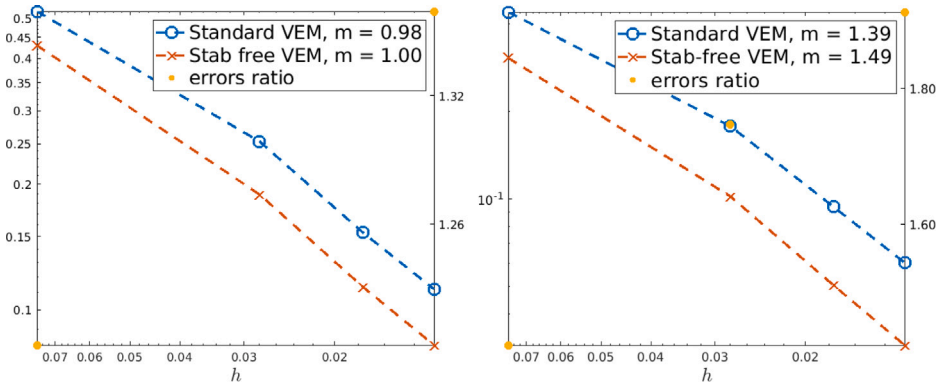

(a) H^1 error (b) L^2 error

Fig. 7. Test with anisotropic diffusivity: convergence plots.

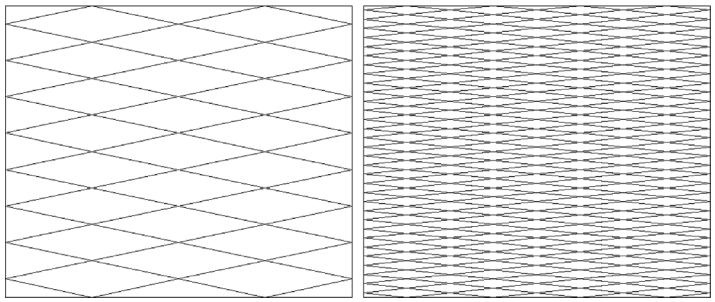

(a) Starting mesh. (b) First anisotropic refinement.

Fig. 8. Test with anisotropic refinement: first two meshes.

sequences, we report the trend of the H^1 and the L^2 errors in Fig. 5 and in Fig. 6. In the legends, we report the computed convergence rates with respect to h, denoted by m. We see that we get the expected values for all the meshes, as obtained in Theorems 5 and 6. The behavior of the H^1 error is similar for the two methods, whereas in the L^2 error we can appreciate a smaller value of the error for the stabilization-free approach. On the right of the panels of Figs. 5 and 6 we report the ratios between the errors corresponding to the standard VEM and the SFVEM.

7.3. Convergence tests on anisotropic problem

In this section, we consider problem (38) where Ω is the unit square, $\mathcal{K} = \begin{bmatrix} 10^{-2} & 0 \\ 0 & 1 \end{bmatrix}$ is an anisotropic diffusivity tensor and $\gamma = 0$. The right-hand side f is defined such that the exact solution is given by $u(x, y) = 10^{-4}xy(1-x)(1-y)(0.5-x)(0.3-y)e^{20x}$. We aim to compare the behavior of standard VEM and SFVEM in terms of energy and L^2 errors, the first one being defined as

$$\text{Energy error} = \sqrt{\sum_{E\in\mathcal{M}_h} \left\| \sqrt{\mathcal{K}} \left(\nabla \Pi_1^{\nabla,E} u - \nabla u \right) \right\|^2_{L^2(E)}}.$$

According to [15], the standard VEM discretization of (38) with $\gamma = 0$ can be given by: find $u_h \in \mathcal{V}_{h,1}$ such that

$$\sum_{E\in\mathcal{M}_h} \left(\mathcal{K}\Pi_0^{0,E}\nabla u_h, \Pi_0^{0,E}\nabla v_h \right)_E + \|\mathcal{K}\|_{L^\infty(E)} S^E \left((I - \Pi_1^{\nabla,E})u_h, (I - \Pi_1^{\nabla,E})v_h \right) =$$
$$\sum_{E\in\mathcal{M}_h} \left(f, \Pi_0^{0,E} v_h \right)_E \quad \forall v \in \mathcal{V}_{h,1}\,. \tag{44}$$

For the proposed method, the discrete formulation is the one presented in (39), using the family of meshes `Polymesher` (Fig. 4(d)). From Fig. 7 we can see that the proposed method performs better in this test case, noting that the L^2 rate of convergence is still pre-asymptotic. This feature of the method was already observed in other similar test cases, see [7,14].

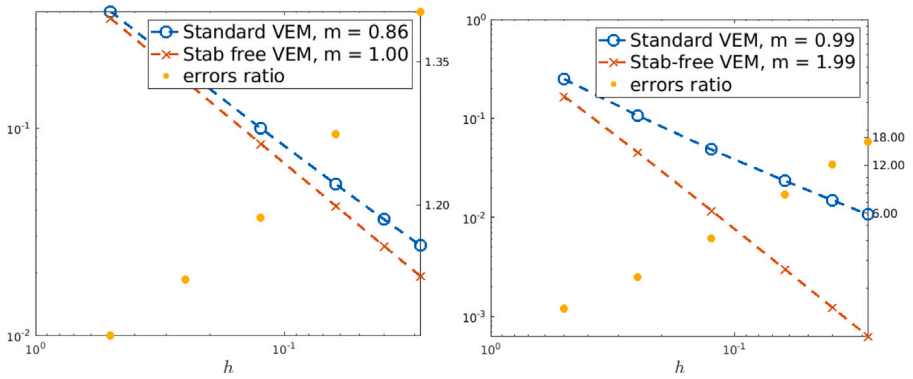

(a) H^1 error (b) L^2 error

Fig. 9. Test with anisotropic refinement: convergence plots.

7.4. Convergence test on anisotropic mesh refinement

To conclude our numerical tests, we consider a test that was performed also in [16], featuring a mesh that is refined following an anisotropic rule. We solve the same problem as in Section 7.2, starting from the mesh in Fig. 8(a), and refining the mesh by a factor α in the horizontal direction and by a factor α^2 in the vertical direction. Fig. 9 shows the convergence plots in the error norms defined above. As observed in [16], the standard VEM method is not properly converging, while the method proposed here exhibits an optimal convergence behavior.

8. Conclusions

We presented a Virtual Element Method whose discrete bilinear form is stabilization-free, in the sense that we do not write it as the sum of a bilinear form involving polynomial projections and a non-operator preserving stabilizing bilinear form. On general quadrilaterals, we proved that such a bilinear form can be obtained by using polynomial projections on the space of curls of harmonic polynomials of degree 2. For more general polygons, we identified a sufficient condition for choosing the degree of the polynomial projection. Moreover, we proposed an algorithm providing the polynomial projection degree ensuring stability. The algorithm requires the computation of edge integrals needed for the construction of the polynomial projection and an incremental local QR factorization. Numerical coercivity tests suggest that choosing locally ℓ_E such that $2\ell_E \geq N_E - 3$ is sufficient for all the shapes. However, the application of the proposed algorithm for polygons without particular shape symmetries leads to a smaller ℓ_E. Numerical results show that the method is especially suitable for solving problems characterized by anisotropic coefficients and solutions and is more robust with respect to anisotropic refinements, whereas in isotropic cases it is equivalent to standard Virtual Elements, usually providing a smaller L^2-error.

CRediT authorship contribution statement

Stefano Berrone: Writing – review & editing, Writing – original draft, Visualization, Validation, Supervision, Software, Resources, Project administration, Methodology, Investigation, Funding acquisition, Formal analysis, Data curation, Conceptualization. **Andrea Borio:** Writing – review & editing, Writing – original draft, Visualization, Validation, Supervision, Software, Resources, Project administration, Methodology, Investigation, Funding acquisition, Formal analysis, Data curation, Conceptualization. **Francesca Marcon:** Writing – review & editing, Writing – original draft, Visualization, Validation, Software, Resources, Methodology, Investigation, Formal analysis, Data curation, Conceptualization.

Declaration of competing interest

The authors declare that they have no known competing financial interests or personal relationships that could have appeared to influence the work reported in this paper.

Data availability

Data will be made available on request.

Acknowledgments

The three authors are members of the Gruppo Nazionale Calcolo Scientifico (GNCS) at Istituto Nazionale di Alta Matematica (INdAM). The authors kindly acknowledge financial support by INdAM-GNCS through Projects 2023 CUP_E53C22001930001, by the Italian Ministry of University and Research (MUR) through the PRIN 2020 project (No. 20204LN5N5_003) and by the European Union through Next Generation EU, M4C2, PRIN 2022 PNRR project CUP: E53D23017950001 and through PNRR M4C2 project of CN00000013 National Centre for HPC, Big Data and Quantum Computing (HPC) CUP: E13C22000990001.

Appendix. Proof of the validity of assumption H.1 for some classes of polygons

In this section, we construct sets of unisolvent degrees of freedom that ensure Assumption **H.1** for particular sets of polygons. In details, we analyze convex polygons, polygons that have only one reentrant corner and an edge lying on the boundary of the kernel of the polygon, and polygons that can be seen geometrically as triangles (with aligned edges). These results are intended to provide sufficient conditions to satisfy Assumption **H.1**.

Proposition 2 (*Convex polygons*). *Let E be a strictly convex polygon with $N_E \geq 5$. In $\mathbb{P}_{N_E-2}(E)$, we have the following degrees of freedom for $p \in \mathbb{P}_{N_E-2}(E)$:*

S.1 For each edge e_i with $i = 1, \dots, N_E - 3$, the moments $\frac{1}{|e_i|}\int_{e_i} pq_j$, for each q_j basis function of $\mathbb{P}_{N_E-1-i}(e_i)$.

S.2 For each edge e_i with $i = N_E - 2, N_E - 1, N_E$, the moment $\frac{1}{|e_i|}\int_{e_i} p$.

*Then assumption **H.1** holds choosing $\ell_E = N_E - 3$.*

Proof. We start by noticing that the total number of degrees of freedom defined in S.1 plus degrees of freedom defined in S.2 equals $\dim\mathbb{P}_{N_E-2}(E) = \frac{N_E(N_E-1)}{2}$. Then, to conclude the proof it is enough to see that a polynomial $p_{N_E-2} \in \mathbb{P}_{N_E-2}(E)$, such that for each edge e_i with $i = 1, \dots, N_E - 3$,

$$\frac{1}{|e_i|}\int_{e_i} p_{N_E-2}\, q = 0 \quad \forall q \in \mathbb{P}_{N_E-1-i}(e_i)\,, \tag{A.1}$$

and for $i = N_E - 2, N_E - 1, N_E$,

$$\frac{1}{|e_i|}\int_{e_i} p_{N_E-2} = 0\,, \tag{A.2}$$

is identically zero in E. In order to prove this, let us consider (A.1) with $i = 1$. This implies that the trace of p on e_1 is zero, then, applying the factorization of polynomials we obtain that $\exists!\ p_{N_E-3} \in \mathbb{P}_{N_E-3}(E)$ such that

$$p_{N_E-2} = r_1 p_{N_E-3}\,, \tag{A.3}$$

where $r_1 \in \mathbb{P}_1(E)$ is such that $r_1(x, y) = 0\ \forall (x, y) \in e_1$. Then, we consider (A.1) with $i = 2$ together with (A.3), obtaining

$$\frac{1}{|e_2|}\int_{e_2} r_1 p_{N_E-3}\, q = 0 \quad \forall q \in \mathbb{P}_{N_E-3}(e_2) \tag{A.4}$$

Since E is a convex polygon, we have that r_1 does not vanish at any internal point of e_2 (being either positive or negative) then the previous relation implies that $\exists!\ p_{N_E-4} \in \mathbb{P}_{N_E-4}(E)$ such that

$$p_{N_E-2} = r_1 r_2 p_{N_E-4}\,. \tag{A.5}$$

Applying the same argument for all the remaining edges considered in (A.1), we obtain that $\exists!\ p_1 \in \mathbb{P}_1(E)$ such that

$$p_{N_E-2} = p_1 \prod_{i=1}^{N_E-3} r_i\,. \tag{A.6}$$

Finally, we notice that (A.2) implies that there exist three points internal to e_{N_E-2}, e_{N_E-1} and e_{N_E} respectively, at which p_{N_E-2} vanishes. Since E is convex, these three points are not aligned and they do not belong to any of the straight lines r_i, $i = 1, \dots, N_E - 3$. Then, p_1 takes zeros at those three points, which implies that $p_1 \equiv 0$ and thus that $p_{N_E-2} \equiv 0$. □

Notice that another set of unisolvent degrees of freedom for $\mathbb{P}_{N_E-2}(E)$ on convex polygons can be found in [26, Theorem 12.1].

The following Proposition states that the degrees of freedom used in Proposition 2 can also be used on polygons with a single angle $\geq \pi$, provided at least one of the edges sees all vertices, i.e. belongs to the boundary of the kernel of the polygon. The degrees of freedom are defined provided the edges are numbered in a particular way. The reader can refer to Fig. A.10 for an example of the numbering of the edges used in the Proposition, in the case of an hexagon.

Proposition 3. *Let E be a non convex polygon with $N_E \geq 5$, having only one internal angle with amplitude $\geq \pi$ and at least one edge lying on the boundary of the kernel of the polygon. Let e_{N_E-2} denote one of such edges, and let e_{N_E-1} and e_{N_E} of the reentrant corner. Then, for a polynomial $p \in \mathbb{P}_{N_E-2}(E)$ we have the following degrees of freedom:*

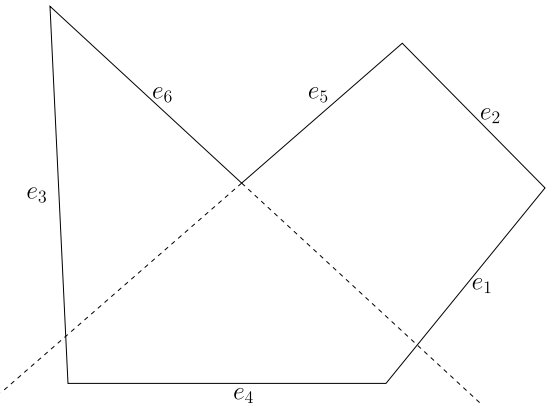

Fig. A.10. Example of a polygon satisfying the hypothesis of Proposition 3. The numbering of the edges is the one used in the Proposition. Here edge e_4 lies on the boundary of the kernel of the polygon, while edge e_5 and e_6 are the ones realizing the non-convexity. The other edges are numbered arbitrarily.

S.1 For each edge e_i with $i = 1, \dots, N_E - 3$, the moments $\frac{1}{|e_i|}\int_{e_i} pq_j$, for each q_j basis function of $\mathbb{P}_{N_E-1-i}(e_i)$.*

S.2 For each edge e_i with $i = N_E - 2, N_E - 1, N_E$, the moment $\frac{1}{|e_i|}\int_{e_i} p$.*

Then assumption **H.1** *holds choosing $\ell_E = N_E - 3$.*

Proof. The proof follows the same steps as the one of Proposition 2. First, if the set of dofs defined by S*.1 is zero for a polynomial $p_{N_E-2} \in \mathbb{P}_{N_E-2}(E)$, then $p_{N_E-2} = p_1 \prod_{i=1}^{N_E-3} r_i$ for some $p_1 \in \mathbb{P}_1(E)$. Now, consider the convex hull of E. $\prod_{i=1}^{N_E-3} r_i$ does not vanish inside e_{N_E-2} because it is on the boundary of the convex hull. Moreover, $\prod_{i=1}^{N_E-3} r_i$ does not vanish inside e_{N_E-1} and e_{N_E} because they are in the interior of the convex hull of E. This implies that $\int_{e_i} p_{N_E-2} = 0$ if and only if p_1 vanishes at three points, each internal to one of e_{N_E-2}, e_{N_E-1}, and e_{N_E}. These three points cannot be aligned because the straight lines defining e_{N_E-1}, e_{N_E} cannot intersect e_{N_E-2} internally, by hypothesis. For example, considering Fig. A.10, we can see that the hull of all straight lines intersecting e_5 and e_6 is the region of the plane above the cone defined by the two dashed half-lines. □

The last result of this section deals with polygons with aligned edges forming a triangle. In the following, $\mathbb{P}_k(\omega)/\mathbb{P}_m(\omega)$ denotes the space of polynomials in $\mathbb{P}_k(\omega)$ that are $L^2(\omega)$-orthogonal to $\mathbb{P}_m(\omega)$.

Proposition 4. *Let E be a polygon with $N_E \geq 5$ such that the minimum number of straight lines necessary to cover ∂E is 3. Then, let η_i $i = 1, 2, 3$ denote the ith geometrical edge of the triangle, $r_i \in \mathbb{P}_1(E)$ be such that $r_i \equiv 0$ on η_i, and let α_i be the number of aligned edges contained in η_i. Let us distinguish three different cases:*

T.1 $\alpha_1 = \alpha_2 = 1$ and $\alpha_3 = N_E - 2$,
T.2 $\alpha_1 = 1$, $\alpha_2 = 2$ and $\alpha_3 = N_E - 3$,
T.3 If $N_E \geq 6$, $1 \leq \alpha_i \leq N_E - 4$ $\forall i$ and $\alpha_1 + \alpha_2 + \alpha_3 = N_E$.

Then for a polynomial $p \in \mathbb{P}_{N_E-3}(E)$, we have the following degrees of freedom:

S^T.1 The internal scaled moments $\frac{1}{|E|}\int_E p\, b$, where $b = r_1 r_2 r_3\, q \in \mathbb{P}_{N_E-3}(E)$, for each $q \in \mathbb{P}_{N_E-6}(E)$ (with $\mathbb{P}_{-1}(E) = \{0\}$),
S^T.2 For each edge $e_i \in \mathcal{E}_E$, the moment $\frac{1}{|e_i|}\int_{e_i} p$,
S^T.3 If T.1:

- *the value of p at the vertex of the triangle given by $\eta_1 \cap \eta_2$,*
- *if $N_E \geq 6$, for each $i = 1, 2$ the moments $\frac{1}{|\eta_i|}\int_{\eta_i} p\, q$, for each q basis function of $\mathbb{P}_{N_E-5}(\eta_i)/\mathbb{P}_0(\eta_i)$.*

If T.2:

- *the value of p at the vertex defined by $\eta_2 \cap \eta_3$,*
- *if $N_E \geq 6$,*
  - *the moments $\frac{1}{|\eta_1|}\int_{\eta_1} p\, q$, $\forall q$ basis function of $\mathbb{P}_{N_E-5}(\eta_1)/\mathbb{P}_0(\eta_1)$.*
  - *the moments $\frac{1}{|\eta_2|}\int_{\eta_2} p\, q$, $\forall q$ basis function of $\mathbb{P}_{N_E-3}(\eta_2)/\mathbb{P}_2(\eta_2)$,*

If T.3:

- *the value of p at the three vertices of the triangle,*
- *the moments* $\frac{1}{|\eta_i|}\int_{\eta_i} p\,q\ \forall q$ *basis function of* $\mathbb{P}_{N_E-3}(\eta_i)/\mathbb{P}_{\alpha_i+1}(\eta_i)$, $\forall i=1,2,3$.

Then assumption **H.1** *holds choosing* $\ell_E = N_E - 4$.

Proof. We start by noticing that the total number of degrees of freedom defined in $S^T.1$, $S^T.2$ and $S^T.3$ equals $\dim\mathbb{P}_{N_E-3}(E) = \frac{(N_E-2)(N_E-1)}{2}$, in all three configurations. To prove the unisolvence of the degrees of freedom for $\mathbb{P}_{N_E-3}(E)$, we first notice that it if $p\in\mathbb{P}_{N_E-3}(E)$ is such that $\gamma^{\partial E}(p)=0$, then $p = r_1r_2r_3q$ for some $q\in\mathbb{P}_{N_E-6}(E)$ and, if

$$\frac{1}{|E|}\int_E p\,b = 0,\ \text{where } b = r_1r_2r_3\,q\,, \forall\, q\in\mathbb{P}_{N_E-6}(E) \tag{A.7}$$

then p is identically zero on E. Then, it is sufficient to prove that the nullity of the dofs defined by $S^T.2$ and $S^T.3$ implies that the trace of the polynomial is null on the boundary ∂E, i.e. $\gamma^{\partial E}(p)=0$. Let us prove it, considering separately the cases T.1, T.2 and T.3.

Case T.1. Let $p\in\mathbb{P}_{N_E-3}(E)$ and assume that all degrees of freedom are zero. By $S^T.2$ we have that for each $e_i\subset\eta_3$, $\frac{1}{|e_i|}\int_{e_i}p=0$. Then there exist N_E-2 distinct points lying on η_3 where p is zero. Then, since $\gamma^{\eta_3}(p)\in\mathbb{P}_{N_E-3}(\eta_3)$, then $\gamma^{\eta_3}(p)\equiv 0$, and in particular $p(\eta_3\cap\eta_1)=p(\eta_3\cap\eta_2)=0$.

Let us consider η_1. By $S^T.2$ and $S^T.3$ conditions, we have that

$$\frac{1}{\eta_1}\int_{\eta_1} p\,q = 0,\ \forall\, q\in\mathbb{P}_{N_E-5}(\eta_1)\ , \tag{A.8}$$

and that p is zero at the endpoints of η_1, then, by polynomial factorization, $\gamma^{\eta_1}(p) = p_2p_{N_E-5}$, where $p_{N_E-5}\in\mathbb{P}_{N_E-5}(\eta_1)$ and $p_2\in\mathbb{P}_2(\eta_1)$ is null at the endpoints of η_1 and positive inside η_1. Conditions (A.8) with $q=p_{N_E-5}$ imply that $\int_{\eta_1}p_2p_{N_E-5}^2=0$, then $p_{N_E-5}=0$ and $\gamma^{\eta_1}(p)=0$. The same argument can be applied for $\gamma^{\eta_2}(p)$. Then p is zero on ∂E.

Case T.2. Let $p\in\mathbb{P}_{N_E-3}(E)$ and assume that all degrees of freedom are zero. By $S^T.2$ we have that for each $e_i\subset\eta_3$, $\frac{1}{|e_i|}\int_{e_i}p=0$. Then, there exist N_E-3 distinct points that lie inside η_3 where p is zero. By $S^T.3$, we also have that p is zero at one of the endpoints of η_3, in particular the vertex $V_{2-3}=\eta_2\cap\eta_3$. Then $\gamma^{\eta_3}(p)=0$. Now, let us consider η_2. Since by $S^T.3$

$$\frac{1}{|\eta_2|}\int_{\eta_2} p\,q = 0\,,\quad \forall\, q\in\mathbb{P}_{N_E-3}(\eta_2)/\mathbb{P}_2(\eta_2)\ , \tag{A.9}$$

then $\gamma^{\eta_2}(p)$ is $L^2(\eta_2)$-orthogonal to $\mathbb{P}_{N_E-3}(\eta_2)/\mathbb{P}_2(\eta_2)$, then $\gamma^{\eta_2}(p)\in\mathbb{P}_2(\eta_2)$. Moreover, considering that for each $e_i\subset\eta_2$

$$\frac{1}{|e_i|}\int_{e_i} p = 0\,, \tag{A.10}$$

which implies that there exists two distinct points inside of η_2 such that p vanishes at that points, together with $p(V_{2-3})=0$, then $\gamma^{\eta_2}(p)=0$. Finally, since we obtain that p vanishes at the endpoints of η_1, and by exploiting $S^T.3$ and $S^T.2$ for η_1, we have

$$\frac{1}{|\eta_1|}\int_{\eta_1} p\,q = 0,\quad \forall\, q\in\mathbb{P}_{N_E-5}(\eta_1)\ , \tag{A.11}$$

using the same arguments as in the previous case, we have that $\gamma^{\eta_1}(p) = p_2p_{N_E-5}$, where $p_{N_E-5}\in\mathbb{P}_{N_E-5}(\eta_1)$ and $p_2\in\mathbb{P}_2(\eta_1)$ is null at the endpoints of η_1 and positive inside η_1. Conditions (A.11) with $q=p_{N_E-5}$ imply that $\int_{\eta_1}p_2p_{N_E-5}^2=0$, then $p_{N_E-5}=0$ and $\gamma^{\eta_1}(p)=0$. Then p is zero on ∂E.

Case T.3. Let $p\in\mathbb{P}_{N_E-3}(E)$, by the conditions in $S^T.3$, we have that for each η_i, with $i=1,2,3$,

$$\frac{1}{|\eta_i|}\int_{\eta_i} p\,q = 0\quad \forall\, q\in\mathbb{P}_{N_E-3}(\eta_i)/\mathbb{P}_{\alpha_i+1}(\eta_i)\ , \tag{A.12}$$

which implies that $\gamma^{\eta_i}(p)\in\mathbb{P}_{\alpha_i+1}(\eta_i)$ for each $i=1,2,3$. Then, applying the condition in $S^T.2$ such that for each edge $e_i\in\mathcal{E}_E$, the moment $\frac{1}{|e_i|}\int_{e_i}p=0$ and the condition in $S^T.3$ such that the value of p is zero at the three vertices of the triangle, then for each η_i there exist α_i+2 distinct points where the value of p is zero. Then p is zero on ∂E. □

References

[1] L. Beirão da Veiga, F. Brezzi, A. Cangiani, G. Manzini, L.D. Marini, A. Russo, Basic principles of virtual element methods, Math. Models Methods Appl. Sci. 23 (01) (2013) 199–214, http://dx.doi.org/10.1142/S0218202512500492.

[2] L. Beirão da Veiga, C. Lovadina, A. Russo, Stability analysis for the virtual element method, Math. Models Methods Appl. Sci. 27 (13) (2017) 2557–2594, http://dx.doi.org/10.1142/S021820251750052X.

[3] M.F. Benedetto, S. Berrone, A. Borio, S. Pieraccini, S. Scialò, Order preserving SUPG stabilization for the virtual element formulation of advection-diffusion problems, Comput. Methods Appl. Mech. Engrg. 311 (2016) 18–40, http://dx.doi.org/10.1016/j.cma.2016.07.043.

[4] S. Berrone, A. Borio, G. Manzini, SUPG stabilization for the nonconforming virtual element method for advection–diffusion–reaction equations, Comput. Methods Appl. Mech. Engrg. 340 (2018) 500–529, http://dx.doi.org/10.1016/j.cma.2018.05.027.

[5] P.F. Antonietti, L. Mascotto, M. Verani, A multigrid algorithm for the *p*-version of the virtual element method, ESAIM Math. Model. Numer. Anal. 52 (2017) 337–364, http://dx.doi.org/10.1051/m2an/2018007.

[6] B. Hudobivnik, F. Aldakheel, P. Wriggers, A low order 3D virtual element formulation for finite elasto–plastic deformations, Comput. Mech. 63 (2019) 253–269, http://dx.doi.org/10.1007/s00466-018-1593-6.
[7] S. Berrone, A. Borio, F. Marcon, Comparison of standard and stabilization free virtual elements on anisotropic elliptic problems, Appl. Math. Lett. 129 (2022) 107971, http://dx.doi.org/10.1016/j.aml.2022.107971.
[8] A. D'Altri, S. de Miranda, L. Patruno, E. Sacco, An enhanced VEM formulation for plane elasticity, Comput. Methods Appl. Mech. Engrg. 376 (2021) 113663, http://dx.doi.org/10.1016/j.cma.2020.113663.
[9] A. Chen, N. Sukumar, Stabilization-free virtual element method for plane elasticity, Comput. Math. Appl. 138 (2023) 88–105, http://dx.doi.org/10.1016/j.camwa.2023.03.002.
[10] A. Chen, N. Sukumar, Stabilization-free serendipity virtual element method for plane elasticity, Comput. Methods Appl. Mech. Engrg. 404 (2023) 115784, http://dx.doi.org/10.1016/j.cma.2022.115784.
[11] B.-B. Xu, F. Peng, P. Wriggers, Stabilization-free virtual element method for finite strain applications, Comput. Methods Appl. Mech. Engrg. 417 (2023) 116555, http://dx.doi.org/10.1016/j.cma.2023.116555.
[12] J. Meng, X. Wang, L. Bu, L. Mei, A lowest-order free-stabilization virtual element method for the laplacian eigenvalue problem, J. Comput. Appl. Math. 410 (2022) 114013, http://dx.doi.org/10.1016/j.cam.2021.114013.
[13] A. Borio, M. Busetto, F. Marcon, SUPG-stabilized stabilization-free VEM: a numerical investigation, Mathematics in Engineering (2024) In press.
[14] S. Berrone, A. Borio, F. Marcon, G. Teora, A first-order stabilization-free virtual element method, Appl. Math. Lett. 142 (2023) 108641, http://dx.doi.org/10.1016/j.aml.2023.108641.
[15] L. Beirão da Veiga, F. Brezzi, L.D. Marini, A. Russo, Virtual element methods for general second order elliptic problems on polygonal meshes, Math. Models Methods Appl. Sci. 26 (04) (2015) 729–750, http://dx.doi.org/10.1142/S0218202516500160.
[16] A. Borio, C. Lovadina, F. Marcon, M. Visinoni, A lowest order stabilization-free mixed virtual element method, Comput. Math. Appl. 160 (2024) 161–170, http://dx.doi.org/10.1016/j.camwa.2024.02.024.
[17] A. Lamperti, M. Cremonesi, U. Perego, C. Lovadina, A. Russo, A Hu–Washizu variational approach to self-stabilized virtual elements: 2D linear elastostatics, Comput. Mech. 71 (2023) 935–955, http://dx.doi.org/10.1007/s00466-023-02282-2.
[18] C. Chen, X. Huang, H. Wei, Virtual element methods without extrinsic stabilization, 2023, arXiv:2212.01720.
[19] A. Russo, N. Sukumar, Quantitative study of the stabilization parameter in the virtual element method, 2023, arXiv:2304.00063.
[20] L. Beirão da Veiga, C. Canuto, R.H. Nochetto, G. Vacca, M. Verani, Adaptive VEM: Stabilization-free a posteriori error analysis and contraction property, SIAM J. Numer. Anal. 61 (2) (2023) 457–494, http://dx.doi.org/10.1137/21M1458740.
[21] S.C. Brenner, L. Sung, Virtual element methods on meshes with small edges or faces, Math. Models Methods Appl. Sci. 28 (07) (2018) 1291–1336, http://dx.doi.org/10.1142/S0218202518500355.
[22] B. Ahmad, A. Alsaedi, F. Brezzi, L.D. Marini, A. Russo, Equivalent projectors for virtual element methods, Comput. Math. Appl. 66 (2013) 376–391, http://dx.doi.org/10.1016/j.camwa.2013.05.015.
[23] D. Boffi, F. Brezzi, M. Fortin, Mixed Finite Elements for Electromagnetic Problems, Springer Berlin Heidelberg, Berlin, Heidelberg, 2013, pp. 625–662, http://dx.doi.org/10.1007/978-3-642-36519-5_11.
[24] L. Beirão da Veiga, F. Brezzi, L.D. Marini, A. Russo, The hitchhiker's guide to the virtual element method, Math. Models Methods Appl. Sci. 24 (08) (2014) 1541–1573, http://dx.doi.org/10.1142/S021820251440003X.
[25] A. Cangiani, G. Manzini, O.J. Sutton, Conforming and nonconforming virtual element methods for elliptic problems, IMA J. Numer. Anal. 37 (3) (2016) 1317–1354, http://dx.doi.org/10.1093/imanum/drw036.
[26] B.D. Bojanov, H.A. Hakopian, A.A. Sahakian, Spline Functions and Multivariate Interpolations, in: Mathematics and Its Application, vol. 248, Springer Dordrecht, 2003, http://dx.doi.org/10.1007/978-94-015-8169-1.
[27] A. Cangiani, E.H. Georgoulis, T. Pryer, O.J. Sutton, A posteriori error estimates for the virtual element method, Numer. Math. 137 (4) (2017) 857–893, http://dx.doi.org/10.1007/s00211-017-0891-9.
[28] C. Talischi, G.H. Paulino, A. Pereira, I.F.M. Menezes, Polymesher: A general-purpose mesh generator for polygonal elements written in matlab, Struct. Multidiscip. Optim. 45 (3) (2012) 309–328, http://dx.doi.org/10.1007/s00158-011-0706-z.